https://doi.org/10.1021/acsnano.9b05579

Selective Modulation Of A1 Astrocytes By Drug-Loaded Nano-Structured Gel In Spinal Cord Injury

*Irma Vismara [1§], Simonetta Papa [1§], Valeria Veneruso [1,2], Emanuele Mauri [2], Alessandro Mariani [3], Massimiliano De Paola [3], Roberta Affatato[4], Arianna Rossetti [2], Mattia Sponchioni [2], Davide Moscatelli [2], Alessandro Sacchetti [2], Filippo Rossi [2], Gianluigi Forloni [1], Pietro Veglianese [1]**

1 Department of Neuroscience, Istituto di Ricerche Farmacologiche Mario Negri IRCCS, via Mario Negri 2, 20156 Milano, Italy;

2 Department of Chemistry, Materials and Chemical engineering "Giulio Natta", Politecnico di Milano, via Mancinelli 7, 20131 Milano, Italy;

3 Department of Environmental Health Sciences, Istituto di Ricerche Farmacologiche IRCCS "Mario Negri", via Mario Negri 2, 20156 Milan, Italy

4. Department of Oncology, Istituto di Ricerche Farmacologiche IRCCS "Mario Negri", via Mario Negri 2, 20156 Milan, Italy

*corresponding author: pietro.veglianese@marionegri.it

§ contributed equally

ABSTRACT

Astrogliosis has a very dynamic response during the progression of spinal cord injury, with beneficial or detrimental effects on recovery. It is therefore important to develop strategies to target activated astrocytes and their harmful molecular mechanisms so as to promote a protective environment to counteract the progression of the secondary injury. The challenge is to formulate an effective therapy with maximum protective effects, but reduced side effects. In this study a functionalized nanogel-based nanovector was selectively internalized in activated mouse or human astrocytes. Rolipram, an anti-inflammatory drug, when administered by these nanovectors limited the inflammatory response in A1 astrocytes, reducing iNOS and Lcn2, which in turn reverses the toxic effect of proinflammatory astrocytes on motor neurons *in vitro*, showing advantages over conventionally administered anti-inflammatory therapy. When tested acutely in a spinal cord injury mouse model it improved motor performance, but only in the early stage after injury, reducing the astrocytosis and preserving neuronal cells.

Spinal cord injury (SCI) is the most frequent disabling injury of the spine. SCI leads to cell degeneration at the epicenter of the lesion, including neurons, astrocytes and oligodendrocytes. [1] Secondary processes (*e.g.* inflammatory response, excitotoxicity, apoptosis and oxidative stress) cause additional loss of neurons and glial cells (secondary injury). The reactive proinflammatory response of the astrocyte population, with the subsequent formation of scar tissue and the inhibition of axonal regrowth, seems to be pivotal. After acute damage, astrocytes become reactive and undergo a spectrum of changes in their phenotype, gene expression and proliferation. [2] It has been suggested that reactive astrocytes near the lesion might have roles that are either beneficial or detrimental in central nervous system (CNS) repair. [1,2] Several neuropathological stimuli induce a variable phenotypic "state" of astrocytes that change after injury. These are commonly called stated A1 and A2 [2,3] and are parallel to the terminology of macrophages M1 and M2, which was applied to the microglial response in the CNS. [4]

Astrocytes with A1 phenotype exert neurotoxic effects, upregulating many genes associated with the synapse and neuronal degeneration, suggesting that A1 has harmful "pro-inflammatory" action. [2,3] In contrast, A2-induced reactive astrocytes exert protective effects by upregulating the expression of neurotrophic factors that promote neuronal survival and regrowth. [2,3]

Various approaches have been employed to counteract the negative effects of activated astrocytes [5], blocking scar formation or pharmacologically and genetically reducing upregulation of axon growth inhibitors. [6–8,9] However, genetic manipulation is not clinically feasible, because ethical issues remain and it could have side effects, whereas pharmacological treatment could act on unwanted common mechanisms without any selective effect on astrocytes. Innovative biomaterial technologies have been developed to induce spinal cord regeneration and improve functional outcomes after injury [10–14]. Polymeric

nanoparticles (NPs) with their versatility in size, potential surface and hydrophilic or lipophilic characteristics, offer considerable advantages in drug delivery, increasing the selectivity of drugs and controlling their release overtime. In the past decade a large number of different NP systems have been tested in SCI, but only a few are directed to astrocytes, and none are selective for them. [6,15,16]

We have focused on a specific category of NPs that, with their ability to swell, are commonly referred to as nanogel (NG). [17] Their advantages, compared with NPs, lie in greater colloidal stability due to higher affinity for water, together with longer retention of their cargo, and easy, reproducible synthesis. [17]

We have now developed and characterized a novel pharmacological delivery tool based on an NG (polyethylene glycol (PEG) and polyethylene-imine (PEI)) coated with primary amines and loaded with a drug (Rolipram) to obtain selective, controlled release for the astrocytic component of the spinal cord.

RESULTS

1. NG synthesis and characterization

NG was synthesized by the CH_2Cl_2-in-water emulsification-evaporation method: "Carbonyldiimidazole (CDI) activated" PEG was dissolved in the organic phase, and PEI was dipped in aqueous solution. After sonication, the progressive evaporation of CH_2Cl_2 in the emulsion status take place. The system can ensure homogeneous dispersion of PEG chains around PEI promoting the interactions among the imidazole and amine moieties of the two polymers, giving rise to the formation of carbamate bonds and entanglement of the chains. Then grafting the terminal amine moieties in already formed NG was done in a single step through the direct addition of 3-bromopropylamine to the NG solution. A reaction scheme for

89 the NG is reported in Figure S1. The 3-bromopropylamine nucleophilic substitution occurred
90 on the residual PEI amine groups and this reaction did not affect the NG bonds, preserving
91 the structural organization of the polymeric chains. The evidence of the system stability after
92 coating relies on the fact that NGs are still present as visible from AFM (Atomic Force
93 Microscopy) (Fig.S2). Carbamate bonds are indeed the crosslinking connections among PEG
94 and PEI chains so, in case of their break, the NG structure would have been no more
95 consistent and the polymers would have been dispersed in the water medium.
96 No competition was observed between this reaction and the NG structural bonds, as
97 demonstrated by the preservation of the corresponding signals in NMR and FT-IR analyses
98 (Fig.S3, S4), after coating. The NG physical features were investigated using dynamic light
99 scattering (DLS) technique: the recorded data of NGs dissolved in PBS on size (diameter) and
100 z-potential are respectively 155 nm (PDI = 0.15) and 3.1 mV. The distributed positive charge
101 was related to the presence of -NH_2 surface groups that gave rise to NG protonation and a
102 positive charged interface.
103
104 ***2. Cellular uptake study of NG in murine astrocytes in vitro***
105 We examined the uptake of biodegradable NG (covalently linked to Cy5) in primary co-
106 cultures of microglia, astrocytes and neurons from the spinal cords of mouse embryos. A
107 specific antibody was used to detect neurons (SMI32) in co-culture with astrocytes; astrocytes
108 and microglia were analyzed in monoculture. “Pro-inflammatory” phenotype was induced by
109 treatment with lipopolysaccharide (LPS) for mono and co-cultures. After 24h exposure to NP,
110 a large amount of NG-based NPs was internalized into the cytosol on the outer nucleus in
111 astrocytes (Fig. 1; A, a). In contrast, when we analyzed activated microglia there were only a
112 few internalized NG (Fig.1; A, b), and none in neurons (Fig.1; A, c). We quantified the

internalized NG as a ratio between the NG signal area and cell area, confirming that a larger amount of NG was taken up by activated astrocytes (Fig.1; A, d).

To confirm the reduced ability to internalize NG, we compared the amount of poly-methyl methacrylate-(PCL), a nanovector selectively internalized in activated microglia [18], and found a significantly lower uptake for NG compared to PCL in the same cells (Fig.1; B, a-e). These data suggest greater tropism of NG for activated astrocytes than microglia or neurons *in vitro*.

Time-lapse analysis was used to investigate the kinetics of internalization of NG in astrocytes. NG uptake was already detectable after 24 hours of treatment, reaching the maximum signal, which did not significantly change three days after the exposure. At five days the NG signal decreased, demonstrating degradation of the nanovector (Fig.1; A, e).

In order to investigate targeting of the NG to activated phenotypes, we compared untreated (CTR) (Fig. S5; A, a, B, a), LPS-treated (Fig. S5; A,B, b) and FGF (A2 stimuli) (Fig. S5; A, c) or IL-4 (M2 stimuli) (Fig. S5; B, c) treated murine astrocytes or microglia in vitro. Quantification of the NG uptake in murine astrocytes and microglia shows higher NG internalization in LPS treated cells compared to CTR and FGF/IL-4 (Fig. S5; A, d, B, d). This suggests a stronger treatment for the proinflammatory phenotype enhancing the selective action.

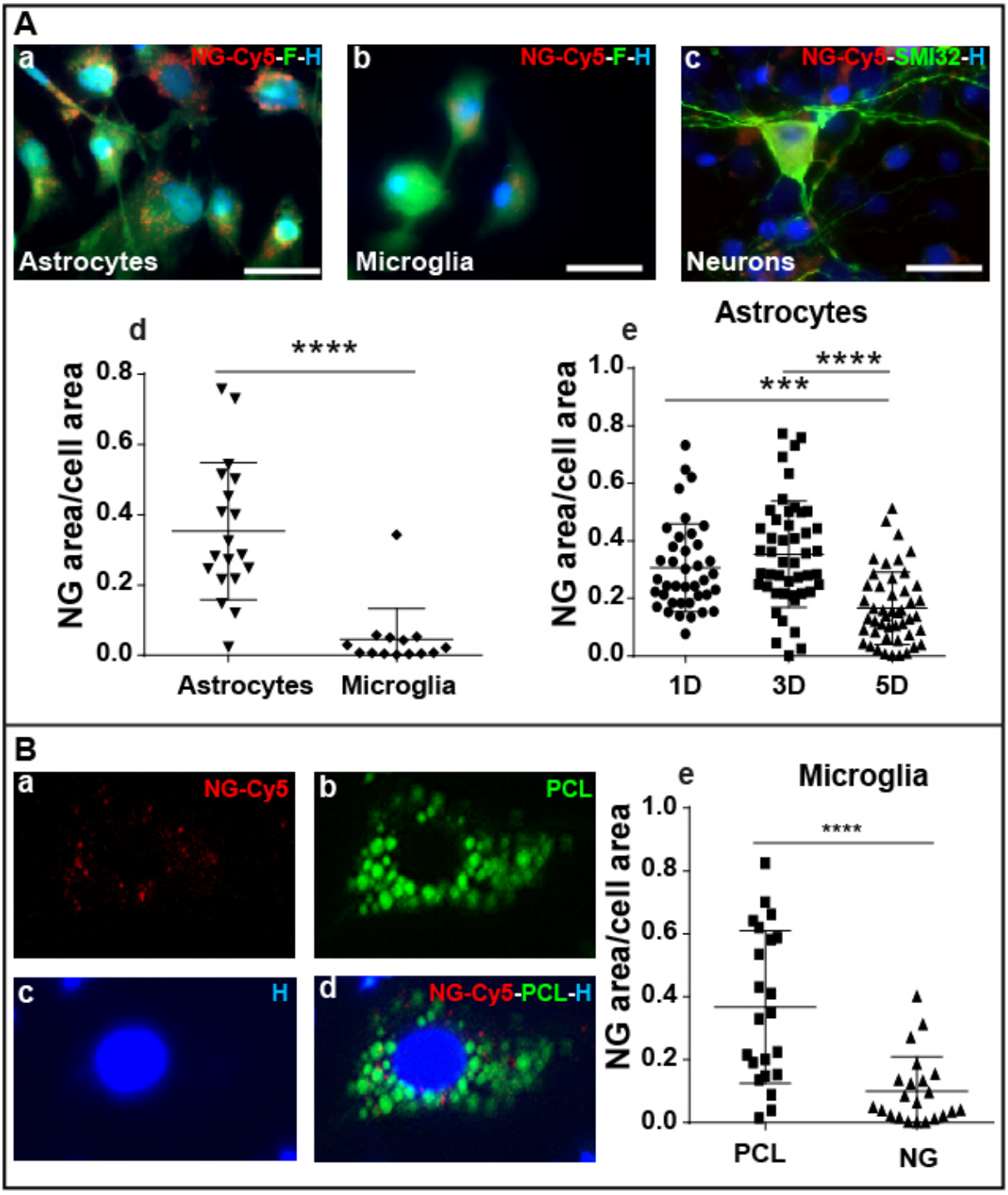

133

134

135

136 ***Figure 1***

137 *A) Characterization of NG uptake in primary cultures of (a) astrocytes, (b) microglia (c)*

138 *neurons. A large amount of NG is located in the cytosol of astrocytes after 1 day (1D) of*

exposure. a) astrocytes or b) microglia stained by fluorescein (F, green); c) neurons stained by SMI32 (SMI32, green); NG conjugated with Cy5 (NG-Cy5, red); cell nuclei stained by Hoechst (H, blue). Scale bar 25 μm. (d) Quantification of the NG uptake in activated astrocytes and microglia shows higher NG internalization in astrocytes. (e) Quantification of NG uptake in astrocytes 1, 3 or 5 days after exposure. At 5 days the NG signal is reduced by degradation of the nanovector.

B) Quantification of NG uptake (a, d, red) vs PCL (b, d, green) in activated microglia. (e) significantly lower uptake was for NG than PCL in activated microglia.

Data are mean ± SD. Mann-Whitney test (A, d, B, e) and one-way ANOVA followed by Bonferroni's post hoc test (A, e). Statistical significance: (***) $p \leq 0.001$; (****) $p \leq 0.0001$.

3. NG internalization and degradation in mouse astrocytes in vitro

To investigate the mechanisms of NG uptake into the astrocytes, we studied NG internalization after 2h pretreatment with chlorpromazine (CPZ, a clathrin-mediated endocytosis inhibitor). Quantification of the NPs in the cytosol showed a significant reduction of the Cy5 signal in CPZ treated astrocytes compared to cells not treated with CPZ (Fig.2; A) suggesting that a mechanism of clathrin-mediated endocytosis was involved in NG uptake. Clathrin-mediated endocytosis can lead to degradation by lysosomes. To study the involvement of lysosomes in the degradation after NG internalization we used a fluorescent indicator (lysosensor, Lys) to test the activity of the lysosomal acidification machinery. Three days after NG exposure we detected evident lysosomal enzymatic activity (fluorescent green signal), closely colocalized with NG (fluorescent red signal) (Fig.2; B, a-c; C, a, b) confirming degradation by lysosomes in astrocytes.

To verify whether the small number of NG in the microglial cells were degraded through lysosomal activity, we studied the colocalization of the NG and Lys signals in microglia. NPs did not show any sign of colocalization with Lys in microglia and in fact the NG signal was dispersed in the cytosol (Fig.2; B, d-f; D, a,b); this was also demonstrated by quantitative analysis where no colocalization was detected with Pearson's coefficient (Fig.2; B, g). This suggests that the amount and mechanism of internalization/degradation in the microglia were different from astrocytes, without any involvement of the clathrin-mediated endocytosis and lysosomal degradation machinery that is instead normally involved in the NP internalization/degradation of microglia.

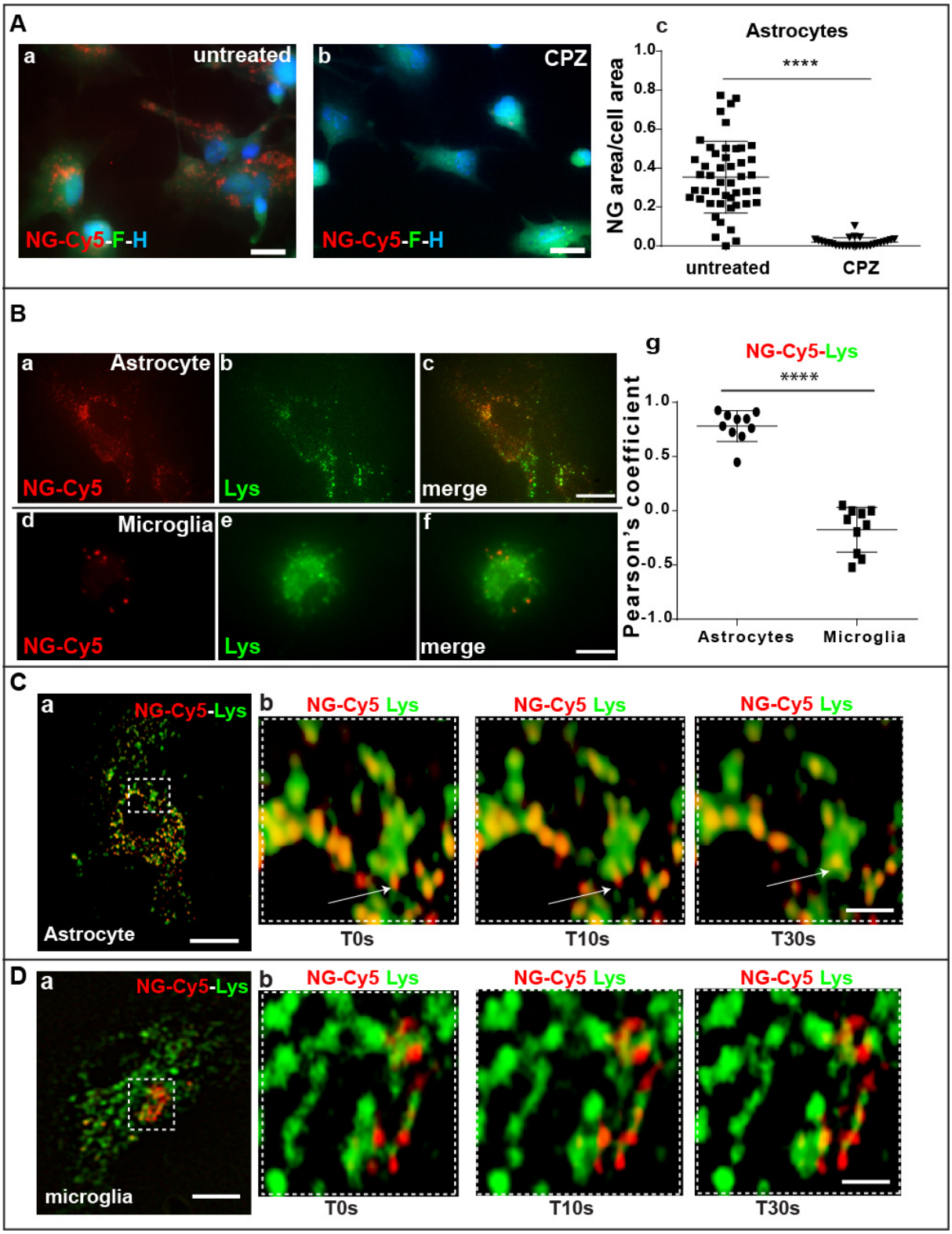
A
a
untreated
NG-Cy5-F-H
b
CPZ
NG-Cy5-F-H
c
Astrocytes
****
NG area/cell area
1.0
0.8
0.6
0.4
0.2
0.0
untreated
CPZ
B
a
Astrocyte
NG-Cy5
b
Lys
c
merge
d
Microglia
NG-Cy5
e
Lys
f
merge
g
NG-Cy5-Lys
****
Pearson's coefficient
1.0
0.5
0.0
-0.5
-1.0
Astrocytes
Microglia
C
a
NG-Cy5-Lys
Astrocyte
b
NG-Cy5 Lys
NG-Cy5 Lys
NG-Cy5 Lys
T0s
T10s
T30s
D
a
NG-Cy5-Lys
microglia
b
NG-Cy5 Lys
NG-Cy5 Lys
NG-Cy5 Lys
T0s
T10s
T30s

Figure 2

A) Pretreatment with chlorpromazine (CPZ) inhibits NG uptake (red) into LPS-activated astrocytes (b) compared to untreated LPS-activated cells (a) stained with fluorescein (F, green) Scale bar A 5 μm.

B) A colocalized signal between NG and the lysosensor indicates that NG is degraded by lysosomal activity in astrocytes (a, b, c). NG (red) showed no colocalization with lysosomes (green) in microglia (d, e, f). This was confirmed by quantitative analysis, using Pearson´s coefficient (g) Scale bar B 15μm.

C) Time-lapse analysis demonstrates colocalization of NG (a, b red) with lysosomes (a, b, green) only in astrocytes (arrow indicates entrapment of NG into a lysosome vesicle during the interval) D) but not in microglia (s=seconds) Scale bar C ,D 3 μm.

Data are mean ± SEM. Mann-Whitney test. Statistical significance: (****) $p \leq 0.0001$.

4. Cellular uptake and degradation study of NG in "iPS-derived" human astrocytes in vitro

To demonstrate that our nanovector-based delivery strategy is applicable in human cells, we treated "iPS derived" human astrocytes with NG. Human astrocytes were prestimulated with LPS for 18 hours then exposed to NP for 24 hours. A large amount of NG-based NPs was internalized in the cytosol, with a distribution comparable to murine astrocytes (Fig. 3 a). Time-lapse analysis was used to record the internalization of NG in human astrocytes. NG was already taken up after 24 hours, reaching the maximum signal, which completely disappeared three days after the exposure (Fig.3 b).

In order to investigate targeting of the NG to activated phenotype, we compared untreated (CTR) (Fig. S5; C, a), LPS-treated (Fig. S5; C, b) or FGF (A2 stimuli) (Fig. S5; C, c) treated human astrocytes in vitro. Quantification of the NG uptake shows higher NG internalization in LPS treated cells compared to CTR and FGF groups (Fig. S5; C, d). This in line with the

treatment of murine astrocytes, where the pro-inflammatory phenotype will receive a stronger treatment.

To demonstrate that the NG degradation was lysosomal as in murine astrocytes, we used the lysosensor to test the activity of the lysosomal acidification machinery. One day after the NG treatment we found remarked lysosomal activity (green fluorescent signal) colocalized with NG (red fluorescent signal) (Fig.3 c,d) and quantified by Pearson´s coefficient (Fig.3 e), confirming that degradation by lysosomes occurred in human astrocytes.

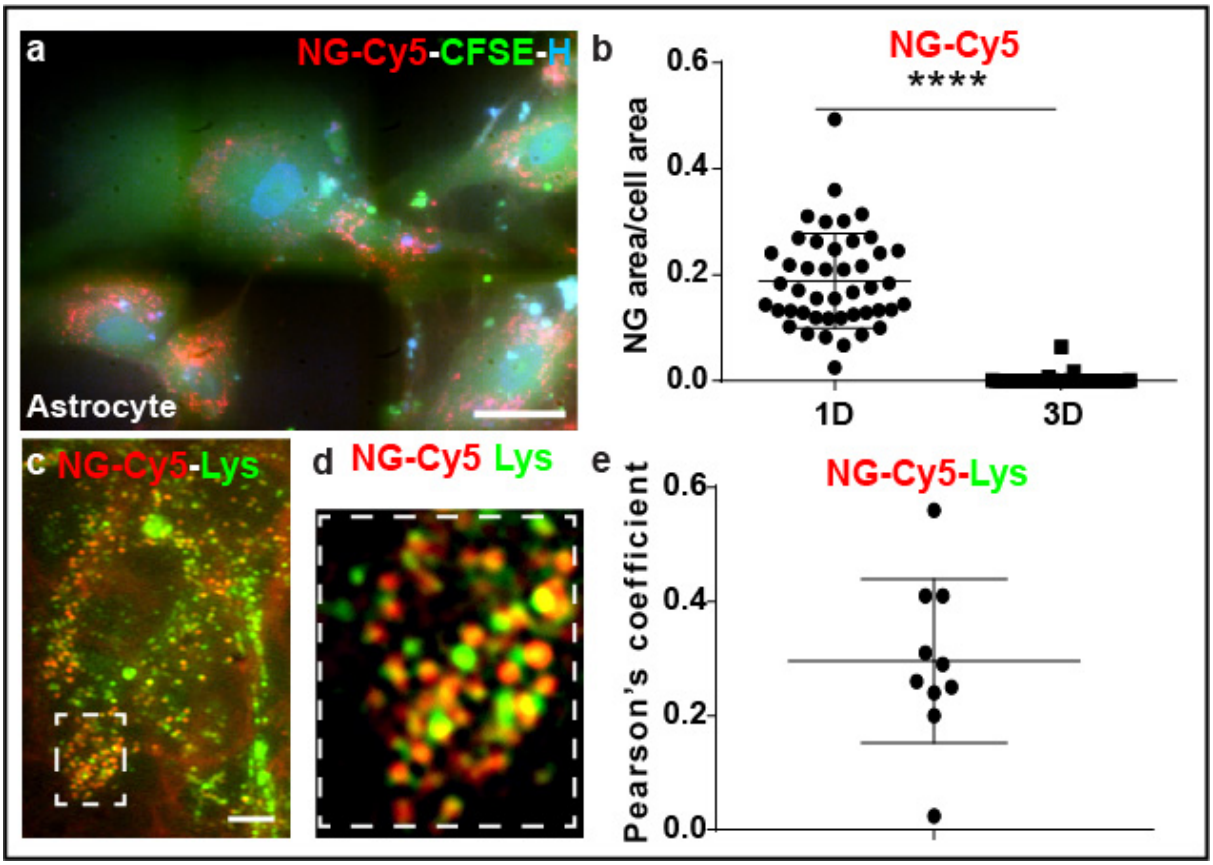

Figure 3

a) NG uptake in iPS human-derived astrocytes. There was a large amount of NG in the cytosol of cells one day (1D) after the exposure. Astrocytes stained by CFSE (green); NG

conjugated with CY5 (NG-CY5, red); cell nuclei stained with Hoechst (H, blue). Scale bar 5µm.

b) Quantification of NG uptake into LPS-activated human astrocytes indicates high NG internalization after one day (1D) of exposure. By three days (3D) NG are completely degraded. Scale bar 2µm.

c,d) Time lapse analysis shows colocalization of the NG signal with the lysosensor (Lys, green), confirming that the nanovector degradation involves lysosomes. Colocalization is quantified by Pearson´s coefficient. Each of the points refers to Lys/NG-RhB signal ratio of individual cells (e). Data are mean ± SEM. Student's T-test. Statistical significance: (****) p ≤ 0.0001. Scale bar 1µm

5. In vitro drug delivery by NG in murine astrocytes

To investigate the ability of NG to deliver molecules into the astrocyte cytosol, NG were loaded with a "drug mimetic" compound (To-pro3, a cell membrane impermeable fluorophore with far-red emission). After 24 hours from exposure to To-pro3-loaded-NG, a clustered signal was seen in the astrocyte cytosol. The colocalization of fluorescent Rhodamine B-positive NG (NG-RhB red signal) with To-pro3 (green signal) showed that the mimetic drug was efficiently encapsulated (Fig.4 a,b,d). In addition to the colocalized signal, a diffused To-pro3 staining was found in the cytosol suggesting that a delivery of this compound occurred (Fig.4 a-d).

To confirm the delivery of To-pro3, we reconstructed the isosurface of the red (RhB-positive NG) and green (To-pro3) signals and quantified their colocalization by Pearson´s coefficient: part of the To-pro3 signal diffused into the cytosol, overlapping RhB-positive NG (Fig.4 e-f). To exclude any free crossing of To-pro3 in cells permeabilized due to damage of the

membrane, we evaluated only viable cells that were also impermeable to propidium iodide, used to test the integrity of the extracellular membrane.

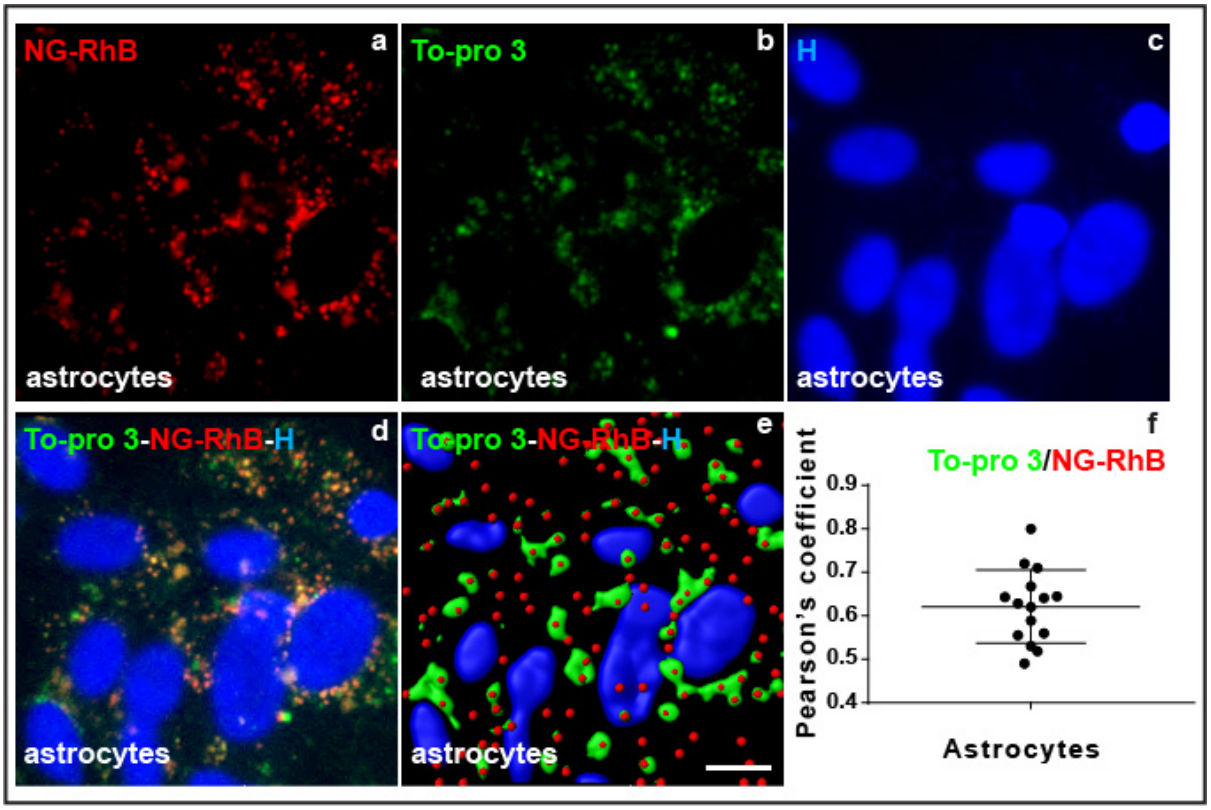

Figure 4

To-pro3 (b, d, e, green) delivery from NG (a, d, e, red) after internalization in astrocytes. Astrocytes give a colocalized signal for To-pro3 and RhB positive NG in the cytosol (a–d). Hoechst was used to stain the astrocyte nucleus (H, blue). A marked diffused signal of To-pro3, not colocalized with NG, is evident in the cytosol of astrocytes five days after NP exposure (d). (e) Isosurfaces reconstruction of the red (RhB-positive NG)/green (To-pro3) signal and (f) quantification of their partial colocalization. Individual data points are referred to To-pro3/NG-RhB signal ratio of individual cells. Scale bar 5µm.

6. Cellular uptake of NG in vivo

To validate and characterize the distribution of NG *in vivo*, we injected the nanovector into the parenchyma of the damaged spinal cord 24h after the trauma (Fig.5 A). The six injections into the spinal cord distributed over a longitudinal distance of 1320± 266 μm (Fig.5 B, a-c). Three days after the injection, we analyzed the tissue to examine the internalization of the NG, with double staining, with markers for astrocytes (GFAP) or microglia (CX3CR1-GFP mice) or neuronal cells (neurotrace), to demonstrate the cellular distribution of the nanovector. Some hypertrophic astrocytes and activated microglial cells were detected in the damaged spinal cord, with an early inflammatory response in the injured site (Fig.5 C, b,c,d,f.g,h). In the epicenter of the lesion NG was mostly internalized into astrocytes, as evident from the colocalization signal of GFAP and Cy5 conjugated with NG (Fig.5 C, a-h); no signal was detected in neurons (Fig.5 D, a-h). Only a few microglia were positive for some NG in the more damaged part of the spinal cord, suggesting that these cells might have more permeabilized membranes (data not shown). These data validated *in vivo* the previous *in vitro* experiments, demonstrating again the diffuse uptake in activated astrocytes in this SCI animal model, whereas internalization was limited in a few microglia, but not in neurons.

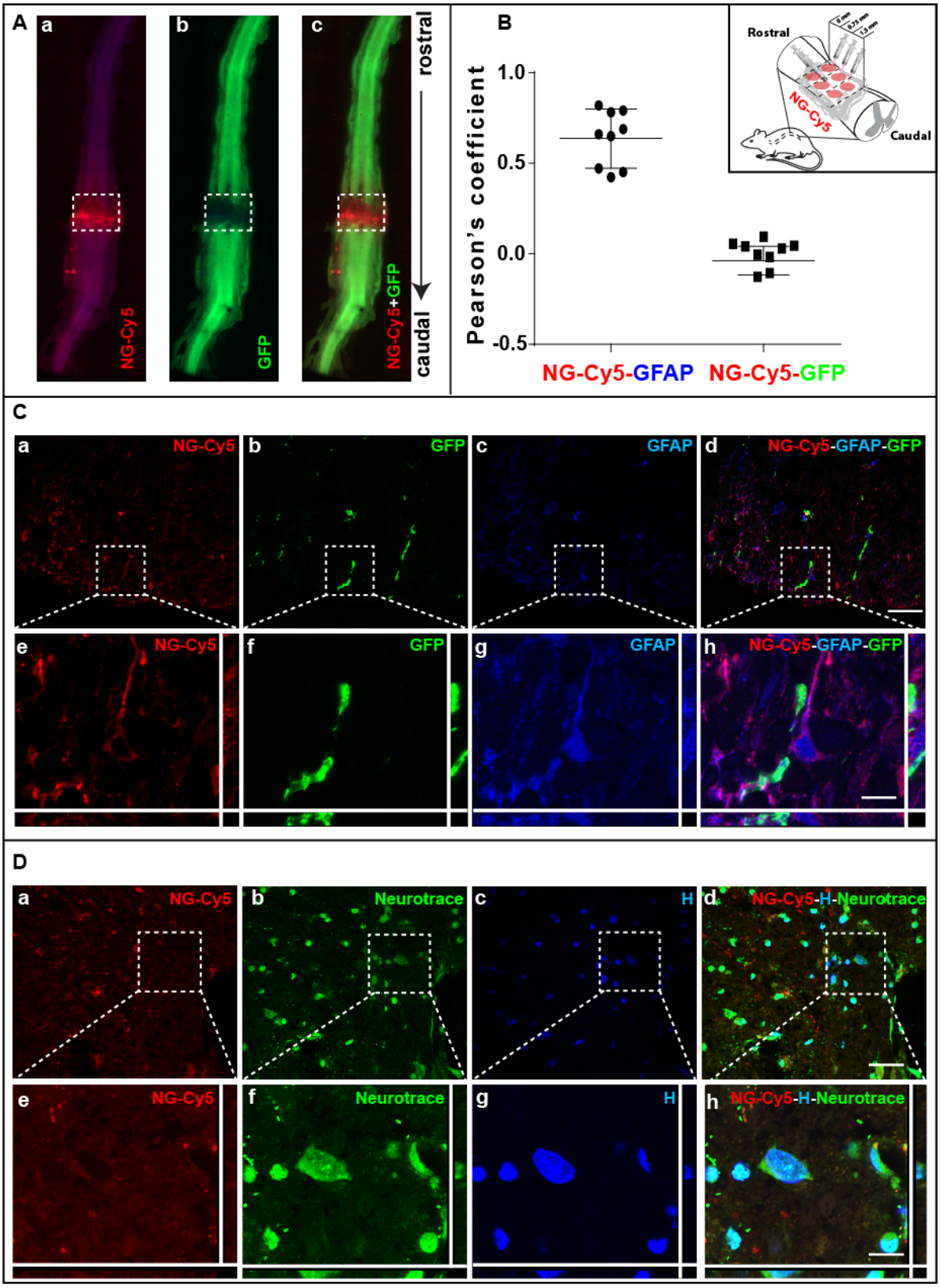
A
a
NG-Cy5
b
GFP
c
NG-Cy5+GFP
rostral
caudal
B
Pearson's coefficient
1.0
0.5
0.0
-0.5
NG-Cy5-GFAP
NG-Cy5-GFP
Rostral
NG-Cy5
Caudal
C
a NG-Cy5
b GFP
c GFAP
d NG-Cy5-GFAP-GFP
e NG-Cy5
f GFP
g GFAP
h NG-Cy5-GFAP-GFP
D
a NG-Cy5
b Neurotrace
c H
d NG-Cy5-H-Neurotrace
e NG-Cy5
f Neurotrace
g H
h NG-Cy5-H-Neurotrace

Figure 5

A) Microscopy of the whole spinal cord 2h after the injection of NG and relative signal amplitude (microglia, CX3CR1 GFP-positive in green; NG-Cy5, red). B) Colocalization analysis quantified by Pearson´s coefficient (nine sampled sections in the site of injection were analyzed). NG-Cy5 markedly colocalized with GFAP, whereas NG-Cy5 vs GFP was much less or no detected. Insert shows NG injections with a distance of 0.75 mm from each other in the lumbar tract of the spinal cord (T12-L1). C,D) High magnification of spinal cord sections show NG internalized into astrocytes (C; a,c,d,e,g,h), but not into microglia (C; a,b,d,e,f,h) or neurons (D; a,b,d,e,f,h). Scale bar C, D 10μm.

7. Pharmacological activity of Rolipram delivered by NG in murine A1 astrocytes in vitro

To demonstrate the ability of NG to deliver functional drugs, we studied Rolipram, an anti-inflammatory drug, acting on the NF-kB pathway in astrocytes *in vitro*. First we characterized the drug release kinetic in vitro. Rolipram is released from NG with a characterized biphasic pattern (Fig. S6). An initial burst release followed by a slower sustained release phase was seen in 14 days (Fig. S6). The percentage of Rolipram released in the first 2 hours (around 30%) can be attributed to the unloaded Rolipram and to the high initial concentration gradient present (Fig. S6).

In order to demonstrate the pharmacological activity, we treated astrocytes with three factors (C1q 400 ng/mL, TNFα 30 ng/mL and IL1α 3ng/mL; hereafter termed pro-inflammatory, PI), that stimulate a specific pro-inflammatory response in astrocytes (A1 status). [2] Rolipram was tested at 0.14 mg/mL, 0.033 mg/mL, 0.023 mg/mL and 0.014 mg/mL (Fig.S7). Real time analysis of the homogenate of astrocytes exposed for 24h with PI showed that inducible nitric oxide synthase (iNOS), a proinflammatory cellular signaling molecule, and Lipocalin 2

(Lcn2), an inducible factor that is secreted by reactive astrocytes, that is toxic to neurons, were significantly higher than in untreated culture (CTR) (Fig.S7). Significant differences were found in the expression of iNOS compared to the CTR when we cotreated astrocytes with PI+Rolipram at the lowest concentration (0.014 mg/mL), whereas co-treatment with Rolipram at higher concentrations (starting from 0.023 mg/mL) was able to counteract the PI status. Significant differences were found for Lcn2 for the highest concentration of Rolipram (0.14 mg/mL) compared to CTR. To demonstrate the ability of NG to load Rolipram and exploit its anti-inflammatory effect, we used the concentration of the drug that had no significant effect on both iNOS and Lcn2. We evaluated 0.014 mg/mL Rolipram loaded into NG, and found that drug internalized by NG reduced iNOS and Lcn2 transcript *in vitro* in PI treated astrocytes compared to PI alone (Fig.6). However, when we tested the single treatment with NG, iNOS was also reduced, but not comparably to Rolipram-loaded NG treatment. This suggests that NG can effectively deliver compounds into activated astrocytes and maximize their pharmacological effects.

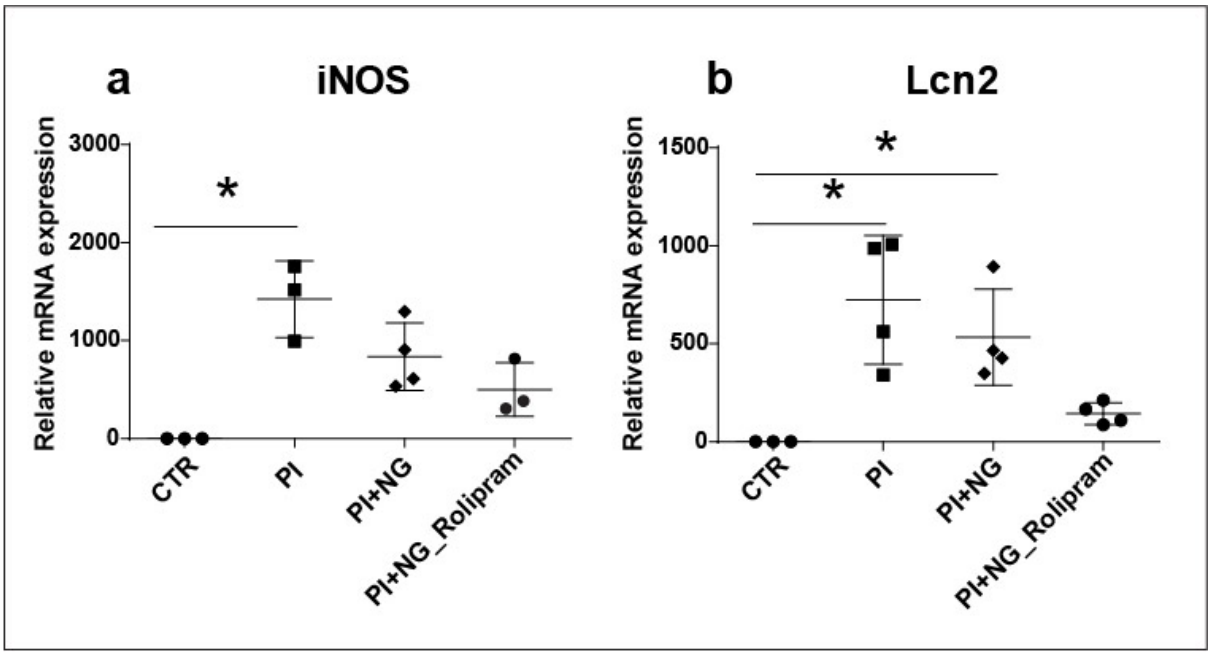

Figure 6

Quantitative mRNA analysis of iNOS (a) and Lcn2 (b) expressed by astrocyte cultures after treatment with PI (C1q, IL1α and TNFα), used as positive control, or PI and NG or PI and Rolipram loaded in NG. Data are mean ± SD. Mann-Whitney test. Statistical significance: (*) $p < 0.05$.

8. Rolipram-loaded NG reverses the toxic effect of proinflammatory murine astrocytes on motor neurons in vitro

We examined whether conditioned medium (CM) from pro-inflammatory astrocytes pretreated with NG or Rolipram-loaded NG improved the damage response on cultured motor neurons. A proinflammatory astrocyte phenotype (A1) was induced by 24h treatment with PI stimuli defined above. [2] Stereology for unbiased cell counting of motor neurons was done after neurofilament immunostaining (SMI32). [19] First, we demonstrated the susceptibility of motor neurons to CM from astrocytes treated for 24h with PI; they showed more - but not significant -, neuronal death after 24h than with control medium (untreated astrocytes, CTR) (Fig.S8 a,b,e). Rolipram-loaded NG (NG 0.0005 mg/mL, Rolipram 0.014 mg/mL) significantly preserved motor neuron viability compared to PI (Fig.S8; b,d,e), whereas NG treatment did not give any significant difference from the PI treated motor neurons (Fig.S8; b,c,e).

To see whether a few internalized NG or NG-Roli found in microglia acted on the pro-inflammatory status of the microglia, we compared CM harvested from untreated microglia (CTR), microglia treated with LPS, microglia co-treated with LPS and NG (LPS-NG) or microglia co-treated with LPS and Rolipram-loaded NG (LPS-NG_Roli) on cultured motor neurons (Fig.S9). We found no differences among the treatments, with comparable amounts of motor neurons. Overall these data suggest that only Rolipram-loaded NG pre-treated astrocytes improve neuronal survival reducing the deleterious inflammatory paracrine effect.

9. Rolipram-loaded NG improves functional recovery only early after SCI in vivo

To test the effect of Rolipram delivered by NG in SCI, we ran *in vivo* experiments. Mice were randomly distributed into three groups and subjected to SCI: untreated (INJ), treated with NG

or Rolipram-loaded NG (NG-Roli) one day post-injury. Six injections with a glass capillary were made into the damaged spinal cord to administer NG (0.025 mg/mL) or NG-Roli (Nanogel 0.025 mg/mL, Rolipram 0.7 mg/mL) (Fig.7 a). We rated behavior with the Basso mouse scale (BMS) weekly up to 35 DPI (Fig.7 b).

In the NG-Roli treated group, there was significant motor functional improvement from 7 to 21 DPI compared to the INJ group (Fig.7 b). After 28 DPI up to 35 DPI motor performance was no longer different from the untreated injured group (Fig.7 b). We also noted a significant behavioral improvement for the NG-Roli treated group compared to the NG group at 7 DPI, that became no longer different from 14 to 35 DPI (Fig.7 b). The NG treated group showed some motor recovery at 21 DPI compared to the untreated injured mice (Fig.7 b). These results suggest that Rolipram had an effect only at 7 DPI after the treatment, in an initial acute-subacute phase, compared to NG treated mice, and from 7 to 21 DPI compared to untreated mice. NG also served to regain partially motor control at 21 DPI, suggesting an effect on astrocytes.

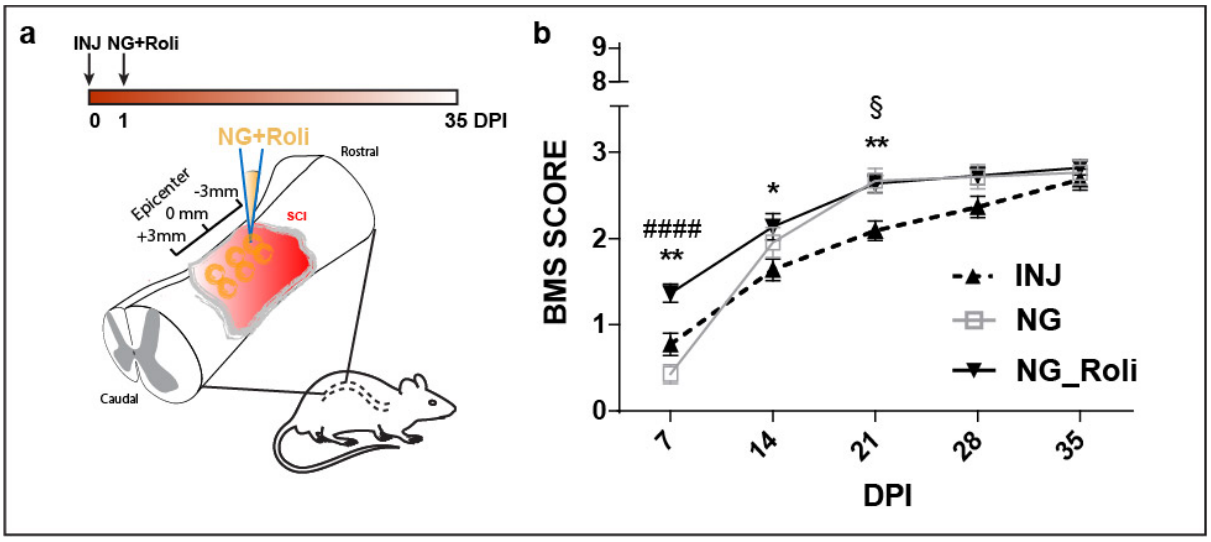

Figure 7

Early treatment with NG loaded with Rolipram improved locomotor performance in SCI mice: a) injection of NG loaded with Rolipram in SCI mice at 1 DPI. b) SCI mice untreated (INJ) or treated with NG (NG) or NG loaded with Rolipram (NG_Roli), examined weekly starting 7 days post-treatment, rated on the Basso Mouse Scale - BMS (score 0, complete paralysis, score 9, complete mobility, compared to healthy mice). Locomotor performance significantly improved in NG_Roli mice compared to the INJ group from 7 to 21 DPI (*) and compared to NG at 7 DPI (#). NG treatment gave significative improvement in locomotor performance at 21 DPI compared to the INJ group (§).

Data are mean ± SEM. One-way ANOVA followed by Bonferroni's post hoc test was applied. Statistical significance: (and §) $p<0.05$, (**) $p<0.01$, (####) $p<0.0001$; N =12 mice/ group.*

10. Rolipram-loaded NG preserved neurons and reduced astrocytosis in vivo

Recovery after treatment with Rolipram-loaded NG was assessed by evaluating neuronal preservation and the level of astrocytosis in the injured spinal cord. We used quantitative stereological analysis to record the number of neurons (NeuN positive cells) (Fig.8 A) and astrocytes (GFAP positive cells) (Fig.8 B) in the tissue. We examined an untreated injured group (INJ) or Rolipram-loaded NG (NG_Roli) treated mice at 14 DPI. An area around the epicenter of the lesion (-1.3/+1.5 mm rostro-caudal) was examined (Fig.8 A, a, B, a). Loss of nervous tissue, impairing recovery ability and functional activity was recorded in the epicenter of the lesion in the INJ group (Fig.8 A, b,d,e). With the NG_Roli treatment, neurons were more preserved, and quantitative analysis indicated a significantly larger number of neurons compared to INJ mice (Fig.8 A,b,c,d,e). Neuronal survival in relation to their distance from the injured epicenter have been showed (Fig.8 A, d). This suggests that more neuronal cells are preserved in the caudal tract that rostral part of the spinal cord.

392

393 Neuronal survival was also investigated at 63 DPI. We analyzed the motor behavior up to
394 63DPI. In this paper we showed up to 35 DPI because from 35 to 63 DPI no difference was
395 found. On the contrary to 14 days post injury, we did not found a significantly difference of
396 neurons by comparing untreated injured mice (INJ) with Rolipram-loaded NG treated mice
397 (NG_Roli) (Fig. S10). This in line with the results in vivo confirming a lack of a long lasting
398 effect of the Rolipram-loaded NG treatment.
399 After injury, astrocytes respond to the lesion, becoming hypertrophic. Activated astrocytes
400 and their paracrine response contribute to scar formation, limiting regeneration of the
401 surviving axons and their functional activity. To demonstrate an effect of the NG_Roli
402 treatment on the response of these cells, we quantified GFAP staining by a stereological
403 approach. There was a significant reduction of hypertrophic astrocytes in NG_Roli treated
404 mice compared to untreated mice in the injured spinal cord (Fig.8 B, b,c,d), as demonstrated
405 by quantitative assessment of the GFAP staining (Fig.8 B, d). The neuronal preservation and
406 the reduced activation of astrocytes correlate with the improvement of motor recovery in the
407 acute-subacute phase after the damage in SCI mice. This suggests that NG_Roli acted on the
408 pro-inflammatory event orchestrated by activated astrocytes (demonstrated here *in vitro*), as
409 well as counteracting the hypertrophic response of the astrocytes following the trauma.
410
411

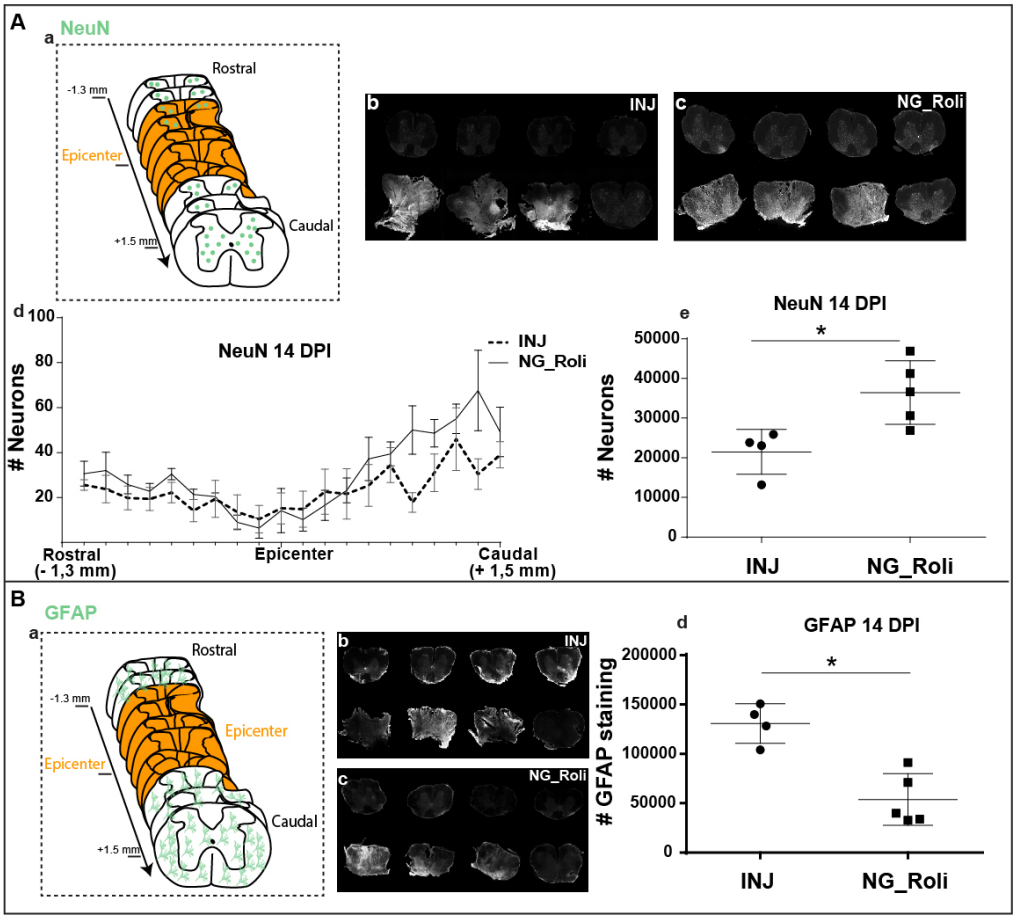

412

413

414 ***Figure 8***

415 *Spinal cord sections stained with NeuN (neuronal marker) (A) or GFAP (astrocyte marker)*

416 *(B) of untreated injured mice (INJ) vs NG-Roli treated mice. Cartoon shows the tract of the*

417 *spinal cord investigated (A,a;B,a). Neuronal survival is showed from the injured epicenter (-*

418 *1.3/+1.5 mm) (A, d). The total number of neurons (A,b,c e) or astrocytes (B, b,c,d) in INJ*

419 *mice compared to the NG-Roli treated group showed a significant proportion of preserved*

420 *neurons and a significant reduction of hypertrophic astrocytes in treated mice. Data are*

421 *mean ± SD. Mann-Whitney test. Statistical significance: (*) p<0.05. N =4/5 mice/ group.*

422

423

DISCUSSION

The importance of the reactive glial cells during the progression of SCI has been recently recognized, but alternative approaches to reduce their pro-inflammatory response, preserving more tissue and neuronal connections after the primary injury, remain a challenge. Our group developed and characterized a selective controlled pharmacologic delivery system for activated astrocytes in the spinal cord based on NP polymers. We tested the selectivity of a nanovector towards the astrocytic component *in vitro* and *in vivo*, and demonstrated its ability to pharmacologically modulate the proinflammatory response of astrocytes after the primary injury. *In vitro* experiments indicated that of a larger amount of nanovectors were internalized into the pro-inflammatory astrocytes compared to A2 stimulated astrocytes. The internalization was mediated by a clathrin-dependent endocytotic pathway, as demonstrated by inhibition after CPZ treatment. Smaller amounts of NG were detected in LPS stimulated microglia, even less in M2 stimulated microglia, and no one in neurons.

After internalization into the cytoplasm of astrocytes, NG undergoes lysosomal degradation releasing the compounds loaded into it (To-pro3 or Rolipram), demonstrating its capacity for internalization, degradation and pharmacological release *in vitro*. Although NG were detected in microglia the amount found was very small, and it seems that the mechanisms of internalization and degradation were different than for astrocytes. NG was not addressed to the lysosome for degradation once internalized in the microglia.

Many types of cells use the clathrin- and caveolae-mediated endocytosis pathways to internalize nanoscale materials. [20,21] These endocytic pathways are the most important ones for the internalization of NP and clathrin-mediated endocytosis with lysosome-oriented degradation was also seen here for astrocytes. The lack of colocalization with lysosomes in microglia suggests alternative uptake mechanisms for NG, such as caveolae-mediated

endocytosis pathways, which avoid lysosomal degradation or clathrin- and caveolae-independent endocytosis. [20]

Microglia also internalize NG differently from other nanovectors previously tested in our group, such as PCL-based NPs that were taken up by clathrin-dependent endocytosis and degraded by lysosomes by the microglia. [18,22] These experiments showed a limited uptake for NG compared to the amount of PCL internalized in activated microglia.

Human iPS cells lend themselves to many applications, but to our knowledge no studies have reported their use to evaluate the delivery ability of nanovectors. We demonstrate that NG, as formulated here, were internalized and degraded in iPS human-derived astrocytes, as demonstrated in murine astrocytes, suggesting potential translability to the clinic.

We also demonstrated *in vivo* and *ex vivo* the validity of NG as a nanovector, whose internalization occurred almost exclusively on astrocytes in the SCI mouse model. Some microglia in the injured site showed a few internalized NG, but very few compared to astrocytes, quite likely because of the effects on the membrane of these cells in the more damaged part of the spinal cord.

The ability of this tool to deliver compounds was further evaluated *in vitro* and *in vivo*, and an anti-inflammatory drug (Rolipram) when administered by NG modulated the response of the astrocytic component by reducing the production of specific inflammatory molecules such as iNOS and Lcn2. CM collected from microglia treated with Rolipram-loaded NG did not influence motor neuron survival. Thus, we can consider the amount of NG internalized into the microglia irrelevant for the treatment.

We also demonstrated that reducing the paracrine inflammatory response of activated astrocytes by Rolipram-loaded NG reversed motor neuron toxicity *in vitro*. The neuroprotective effect was detected in the acute-subacute phase after the lesion and confirmed by motor functional improvement from 7 to 21 DPI. NG treatment alone also served to

partially regain motor control at 21 DPI. NG treatment *in vivo* suggests an effect on astrocytes due to the polymeric structure, but this requires further study. We also showed *ex vivo* that Rolipram-loaded NG preserved neurons and reduced astrocytes at 14 DPI; these neurons were not preserved at 63 DPI, supporting the behavioral findings.

The post-injury astrocyte response is recognized an important contributor to functional recovery after traumatic SCI. [23,24] Recent studies have made important progress in astrogliosis after CNS injuries, identifying specific roles and marker genes for different astrocyte subtypes. [3,23–25] Astrocytes activated by molecular mediators released in the environment, acting as pro-inflammatory or anti-inflammatory stimuli [3], in turn play an important role in the inflammatory response. [3] Reactive astrocytes after activation increase GFAP[1,2,26] and release many molecules. One of them, Lcn2, can promote neuronal death [27,28] and acts as an inflammatory molecule contributing to the secondary injury damage in SCI. [27] In the chronic phase, the reactive astrogliosis lead to extracellular matrix deposition and formation of glial scar. [1,26]

Here we demonstrated that a nanovector tool such as NG can treat pharmacologically activated astrocytes with an anti-inflammatory drug (Rolipram), to reduce the amount of Lcn2 and iNOS produced by these cells. The secretion of Lcn2 and iNOS contributes to inflammation in many CNS pathologies, including SCI. [27,29] iNOS produces a large amount of NO that causes pathological changes in various biological substrates (peroxidation of the cellular lipid components), resulting in cellular damage. [29] Lcn2 secreted by astrocytes further sustains inflammation which in turn promotes neuron death. [27,28,30] Lcn2 is activated by signaling pathways such as NF-kB or STAT3. [31–33] We found that Rolipram acted on NF-kB to reduce the mRNA levels of Lcn2 and concomitantly iNOS, potentially limiting the negative effect of a pro-inflammatory response of astrocytes. Deletion of Lcn2 limits the pro-inflammatory phenotypes of activated astrocytes *in vitro* and *in vivo* [30,34], giving greater

recovery in mouse models of SCI. [27] Lcn2 knock-out mice had consistent neuronal survival and myelin sparing after SCI. [27] Acting on iNOS and Lcn2 looks like a promising therapeutic approach that could be associated to other treatments to strengthen the effect.

CONCLUSION

Different nanovectors are internalized into astrocytes, but none in a selective way for treating the astroglial pro-inflammatory response. [35] Because astrogliosis is closely interlaced and dynamic depending on the injury phase, it may have beneficial or detrimental effects on SCI recovery. It is important therefore to develop strategies to target individual cellular and molecular mechanisms. This study demonstrated the selective efficacy of Rolipram delivered by biodegradable NG in limiting the pro-inflammatory response mediated by astrocyte activation in a mouse model of SCI, but other diseases with an astrocyte-based glial response may gain too from this selective therapeutic approach. This delivery strategy could also be considered for other molecules able to promote neuroprotective astrocytes (A2 phenotype), opening the way to a new cell-specific therapeutic treatment to ameliorate SCI and other neurological diseases.

MATERIALS AND METHODS

NANOGEL DESIGN AND CHARACTERIZATION

The experimental procedures required the following polymers in the nanogel (NG) design: polyethylene glycol 8000 (Mw 8 kDa, from Merck KGaA, Darmstadt, Germany) and linear polyethyleneimine 2500 (Mw 2.5 kDa, from Polysciences Inc., Warrington, USA). All other chemicals were purchased from Merck (Merck KGaA, Darmstadt, Germany) and used as received, without any further purification. Solvents were of analytical-grade purity. All the Cy-5 derivatives were stored at -20°C.

NG was synthesized according to this procedure: PEG hydroxyl groups were modified with imidazole moieties and PEI functionalized with Cy5 (molar ratio PEI:Cy5 1:0.025) using copper-catalyzed azide-alkyne Huisgen cycloaddition (CuAAC) reaction. Then two solutions were prepared separately: in the first, the resulting PEG (200 mg, 0.025 mmol) was dissolved in CH_2Cl_2 (3 mL), and the second one was obtained by dissolving PEI conjugated Cy5 (52 mg, 0.017 mmol) in distilled water (5 mL). The organic solution was added dropwise to the aqueous system, under vigorous stirring, and the final mixture was sonicated for 30 min. The polymeric mixture was then stirred for 17 h at 25°C (room temperature, r.t.) with the gradual evaporation of CH_2Cl_2. This aqueous system was purified by dialysis against slightly acid water and lyophilized, resulting in a green solid.

The primary amines were grafted around the NG surface. NG (15 mg, 0.566 mol) were dissolved in distilled water (1 mL) and kept under stirring at r.t. 3-bromopropylamine hydrobromide, the chemical carrying -NH2 groups, (4.95 mg, 22.64 μmol) was dissolved in distilled water (0.5 mL) and added dropwise to the NG solution. The mixture was stirred for 17h, in the dark, at r.t.

539 Dialysis against distilled water (1000 mL) using a regenerated cellulose membrane (MW cut-
540 off 6-8 kDa) was done for two days, with daily water exchange, to remove unreacted species
541 and any by-products. The system was frozen at -80°C and the product was recovered by
542 lyophilization. These NG coated with primary amine moieties will be indicated as NG.
543 Polymer functionalizations were evaluated by NMR and FT-IR analyses. 1H-NMR spectra
544 were run on a Bruker AC (400 MHz) spectrometer, using deuterated chloroform (CDCl3) for
545 PEG and NG samples, and deuterium oxide (D_2O) for PEI derivatives as solvents, and
546 chemical shifts were reported as δ values in parts per million, tetramethylsilane (TMS) as
547 internal reference. FT-IR spectra were recorded using the KBr pellet technique for the
548 analyzed samples and a Thermo Nexus 6700 spectrometer coupled to a Thermo Nicolet
549 Continuum microscope equipped with a 15× Reflachromat Cassegrain objective, at r.t. in air
550 in the wave range 4000–500 cm^{-1}, with 64 accumulated scans and a resolution of 4 cm^{-1}. The
551 nanogel size, polydispersity index (PDI) and z-potential were recorded using Dynamic Light
552 Scattering (DLS) and a Zetasizer Nano ZS from Malvern Instruments. The samples were
553 dissolved in distilled water and the solution was equilibrated for 60 s before data analysis at
554 37°C. Data are the mean of three measurements for each NG. NG dimensions were studied
555 with Atomic Force Microscopy (AFM). The samples were prepared by dropping nanogel
556 latexes onto silicon substrate and then drying. AFM images on 1 × 1 μm areas were recorded
557 for the preliminary morphologic evaluation; 500 × 500 nm images were cropped and a height
558 line profile was drawn for each single gel. Surface morphology was evaluated by flattening
559 the images (first order) using NTMDT software.
560
561 *PRIMARY CELL CULTURES*

562 Primary cultures of microglia, astrocytes, or astrocyte/neuron co-cultures were obtained from
563 the spinal cord of 13-days-old C57BL/6J mouse embryos (Charles River Laboratories
564 International, Inc.) by adapting protocols previously described [36].
565 Ventral horns were isolated from the embryonic spinal cord and treated with DNAse and
566 trypsin (Sigma-Aldrich). After centrifugation using a cushion of bovine serum albumin
567 (BSA), a mixed population of neurons/glia was obtained. A second centrifugation (800 x g for
568 15 min) was done through a 6% iodixanol pillow (OptiPrepTM; Sigma-Aldrich). At the top of
569 the iodixanol pillow a narrow band was obtained, corresponding to the fraction enriched with
570 motoneurons, and a yellow pellet. The glial feeder layer was prepared by plating the glial
571 fraction at a density of 25,000 cells/cm2 in flasks pre-coated with poly L-lysine (Sigma-
572 Aldrich).
573 From the flask containing confluent mixed glial cultures, purified microglia were obtained
574 after shaking at 275 rpm overnight in incubators. The floating cells (mostly microglia) were
575 collected and seeded at a density of 40,000 cells/cm2 on poly-L-lysine pre-coated 24-well
576 plates.
577 To obtain astrocyte-enriched cultures, glial cultures from which the microglia had previously
578 been collected were treated with 60 mM L-leucine methyl ester (Sigma-Aldrich) for 90
579 minutes. To derive purified cultures and to establish a glial feeder layer for neuron/astrocyte
580 co-cultures, the astrocytes were collected and seeded at a density of 40,000 cells/cm^2 on 24-
581 well plates pre-coated with poly-L-lysine.
582 Finally, to establish neuron/astrocyte co-cultures, the motor neuron-enriched fraction (from
583 the iodixanol-based separation) was seeded at a density of 15,000 cells/cm^2 onto a mature
584 astrocyte layer. In these co-cultures, about 84±5% of the neurons were SMI32-positive, with
585 the typical motor neuron morphology, as previously reported. [36]
586

IPSc-DERIVED ASTROCYTE CULTURES

Episomal human iPSC (hiPSC) were obtained from GibcoTM (Life Technologies, CA, US, Lot V2.0). The hiPSC line was cultured and expanded in feeder-free conditions by passaging every 3–5 days when they reached 70–80% confluence in a xeno-free culture medium formulation (StemMACS™ iPS-Brew XF, Miltenyi Biotec S.r.l.). Neural stem cells (NSC) were derived from hiPSC using a commercial manufactured culture medium in a monolayer protocol [37]. Briefly, hIPSCs cultured in feeder-free conditions were split into six-well plates in a 1:3 ratio. The day after plating, culture medium was replaced with Gibco PSC Neural Induction Medium (Life Technologies) containing Neurobasal medium and Gibco PSC neural induction supplement. On day seven of neural induction, primitive NSCs (pNSCs) were dissociated with Accutase (Life Technologies), passed through a 100-μm strainer and plated on Geltrex-coated dishes at a density of 0.5–1x10^5 cells/cm^2 in an NSC expansion medium, composed Neurobasal medium and Advanced DMEM/F12 (1:1), with 2% neural induction supplement. NSC were expanded for different passages before the induction of astrocyte differentiation.

To obtain differentiated astrocyte cultures, dissociated pNSCs in the sixth through the tenth passage (P6-10) were plated onto Geltrex-coated 24-well plates at a density of 5x10^4 cells/ cm^2 in an astrocyte differentiation medium (DMEM supplemented with 1% N2, Glutamax and fetal bovine serum (FBS); Life Technologies) for twenty-one days.

On the day twenty-one of astrocyte differentiation, cultures were exposed to LPS (10 ug/mL) for 18h or A1 phenotype was induced by treatment with FGF (100 ng/mL) for 18h in medium with 10% serum. Empty NG was then added to activate cultures and time-lapse analysis was done for up to three days to establish the degradation time of NG. To assess the NG degradation by lysosomes, human astrocytes were marked with Lyso sensor dye (1:20.000 dilution, Life Technologies, cat. n. L7535) 24h after exposure. Culture samples were

612 processed in parallel to verify the expression of astrocyte markers and the absence of stem
613 cells.
614
615 *CULTURE TREATMENTS*
616 Microglia activation was induced by exposing purified microglia cultures to 1 μg/mL of LPS
617 (from Escherichia coli 0111:B4; Sigma-Aldrich), as previously reported [36], or IL-4 10 ng/mL
618 for 18h. The murine astrocytes was activate by LPS 1 μg/mL, A1 phenotype was induced by
619 treatment with C1q 400 ng/mL, TNFα 30 ng/mL, IL1α 3 ng/mL for 24h [3] and A2 phenotype
620 was induced by treatment with FGF (100 ng/mL) for 18h. Empty NG, NG loaded with
621 Rolipram loaded with To-pro3, or free Rolipram, were then added to the activated cultures.
622 To investigate NG uptake, we treated astrocytes with chlorpromazine hydrochloride (CPZ;
623 Sigma-Aldrich), CPZ (40 μM) 2h before NG exposure.
624 Astrocyte/neuron co-cultures were treated with CM from microglia or astrocytes incubated
625 with different treatments for 24h: after microglial activation, cells were incubated with fresh
626 medium or NG or NG loaded with Rolipram for 24h, while astrocytes were induced toward
627 A1 and treated with NG or NG loaded with Rolipram for 24h. At the end of the treatment,
628 motor neuron cultures were stained with SMI-32 antibody (Biolegend; 1:1000) and
629 stereologically counted (see below).
630
631 NG INTERNALIZATION
632 To quantify the internalization of NG in murine and human cells, images were randomly
633 selected and acquired 24h, three and five days after the NG exposure with a Cell R
634 microscope (Olympus) equipped with 60X magnification and an ORCA camera
635 (Hamamatsu).

The fluorescent signal was quantified using the free Fiji software (http://fiji.sc/Downloads). The NG signals in single cells (about 30-50) were evaluated as the ratio between the Cy5 signal area and the cell area. To overcome the limits associated with a change of the shape seen after treatment with FGF (for in vitro astrocytes) or IL-4 (for in vitro microglia) we investigated the NG signal for single cells (region of interest determined by fluorescein staining) for comparing these treatments.

REAL TIME RT-PCR

Total RNA was extracted from astrocytes or microglial cultures using a miRNeasy Mini Kit (Qiagen, Valencia, CA, USA). Briefly, cells were collected in QIAzol Lysis Reagent and lysed with a pipette. Chloroform was added to the homogenate and a phase extraction was done. A small volume of the aqueous phase (0.3 mL) was added to 450 mL of ethanol and loaded onto an RNeasy column. The column was washed and RNA eluted following the manufacturer's recommendations. RNA was quantified by a spectrophotometer at 260 nm for all samples. To remove any contaminating genomic DNA, total RNA was digested with DNase (Applied Biosystems) and reverse-transcribed with random hexamer primers using Multi-Scribe Reverse Transcriptase (Taq-Man Reverse transcription reagents; Applied Biosystems). Realtime RT-PCR was run using 4 uL of cDNA, 200 nmol of each primer and SYBR Green chemistry (Applied Biosystems) in a total volume of 22 uL. After completion of qPCR, a melting curve of amplified products was plotted. Data were collected using the SYBR Green fluorescence during Real-Time RT-PCR on an Applied Biosystems 7300 system. The expression of the following genes was analyzed:

iNOS (Fw: GACGAGACGGATAGGCAGAG; Rev: GTGGGGTTGTTGCTGAACTT)

Lcn2 (Fw: TTTGTTCCAAGCTCCAGGGC; Rev: TGGCGAACTGGTTGTAGTCC)

β-Actin (Fw: CGCGAGCACAGCTTCTTT; Rev: GCAGCGATATCGTCATCCAT)

β-Actin was used as the reference gene and relative expression levels were evaluated according to the manufacturer's DDCt method (Applied Biosystems). Data are expressed as the fold change from uninjured spinal cord (healthy condition).

IMMUNOCYTOCHEMISTRY

Motor neurons were fixed with 4% paraformaldehyde for 40 min then incubated for 1h at r.t. in the blocking solution (PBS, 0.2% Triton X-100 (Sigma-Aldrich) and 1% FBS (Sigma Aldrich). Anti-SMI-32 primary antibody (mouse; BioLegend) was diluted (1:1000) in PBS and incubated at r.t. for 4h. The sections were washed with PBS and the appropriate fluorescent secondary antibody was diluted in PBS and incubated for 1h at r.t.

CELL STAINING

Cells were fixed with 4% paraformaldehyde for 40 min and stained with Fluorescein (0.1 ug/mL; Sigma-Aldrich) for 30 min at r.t. For evaluation of live cells, they were incubated with CellTraceTM CFSE Cell proliferation kit (1:1000 dilution, Life Tecnologies, cat n.C34554) for 30 min. To measure lysosomal activity we used lysosensor dye (1:20.000 dilution, Life Technologies, cat. n. L7535). Cell nuclei were labeled with Hoechst 33258 (Invitrogen) by incubation with a 250 ng/mL solution.

NUMBER OF MOTOR NEURONS IN VITRO

Images of the entire wells were acquired with a Cell R microscope (Olympus) equipped with an ORCA camera (Hamamatsu) using a mosaic imaging protocol with 20X magnification. For frame sampling a grid (1000*1000 μm single frame) was superimposed on the images and alternate frames were examined with stereological probes (unbiased fractionator probe

686 dimension, 307*235 μm). The total number of motor neurons was calculated with the
687 following formula: N =ΣQ * 1/asf*1/ssf, where Q was the number of neurons counted in the
688 frame, the area probe 307*235μm, the area frame 1000*1000 μm, asf (area probe/area
689 frame), and ssf (sampling fraction of every 2nd frame). Intra-animal coefficient of error (CE)
690 and inter-animal coefficient of variation (CV) for neuronal counts [38,39] were calculated as
691 follows: mean CE for co-culture motor neurons/astrocytes treated with PI and astrocyte
692 conditioned medium: CTR-CM 0.082, PI 0.080, PI-NG 0.058, PI-NG-Roli 0.071. CV: CTR-
693 CM 0.243, PI 0.126, PI-NG 0.343, PI-NG-Roli 0.197. Mean CE for co-culture motor
694 neurons/astrocytes treated with PI and microglia conditioned medium: CTR-CM 0.075, PI
695 0.068, PI-NG 0.075, PI-NG-Roli 0.073 and CV: CTR-CM 0.178, PI 0.216, PI-NG 0.197, PI-
696 NG Roli 0.300.
697
698 *ANIMAL CARE*
699 The IRCCS adheres to the principles set out in the following laws, regulations, and policies
700 governing the care and use of laboratory animals: Italian Governing Law (D.lgs 26/2014;
701 Authorisation n.19/2008-A issued March 6, 2008 by Ministry of Health); Mario Negri
702 Institutional Regulations and Policies providing internal authorization for persons conducting
703 animal experiments (Quality Management System Certificate – UNI EN ISO 9001:2015 –
704 Reg. N◦ 6121); the NIH Guide for the Care and Use of Laboratory Animals (2011 edition) and
705 EU directives and guidelines (EEC Council Directive 2010/63/UE). The Statement of
706 Compliance (Assurance) with the Public Health Service (PHS) Policy on Human Care and
707 Use of Laboratory Animals was been recently reviewed (9/9/2014) and will expire on
708 September 30, 2019 (Animal Welfare Assurance #A5023-01).
709
710 *SURGERY*

C57BL/6J mice (Charles River Laboratories International, Inc.) or B6.129P-Cx3cr1tm1Litt/J mice (The Jackson Laboratory) were used for *in vivo* studies. Before surgery, the animals received an antibiotic and analgesic, with respectively subcutaneous injection of ampicillin (50 mg/kg) and buprenorphine (0.15 mg/kg). The entire surgical procedure was carried out in deep anesthesia under ketamine hydrochloride (IMALGENE, 100 mg/kg) and medetomidine hydrochloride (DOMITOR, 1 mg/kg) intraperitoneally. Animals were placed on a Cunningham Spinal Cord Adaptor (Stoelting, Dublin, Ireland) mounted on a stereotaxic frame, and laminectomy of the T12 vertebra was done to uncover the lumbar spinal cord. Mechanical trauma of the spinal cord at T12 was induced using an Mann-Whitney test with a closing force of 30g (left in place for 1 min, then removed). After spinal cord compression, dorsal muscles were juxtaposed using absorbable sutures and the skin was sutured. Two hours (for NG distribution experiment) or one day (for behavioral evaluation) after surgery, the spinal cord of SCI mice was exposed and injected intraparenchymally with NG, NG-Cy5 loaded with Rolipram or free Rolipram. Six 0.250 uL injections were done with a glass capillary (outer diameter 40±2 μm), to cover the injured area. The capillary was positioned ±0.5 mm from the midline, then it was deepened into the parenchyma to 0.6 mm below the pia mater. After treatment, dorsal muscles were juxtaposed using absorbable sutures and the skin was sutured and disinfected.

BEHAVIORAL EVALUATIONS

Mice after SCI were evaluated by testing hind-limb locomotor performances using the Basso Mouse Scale (BMS) once a week from seven to thirty-five DPI. The BMS is a 10- point scale (9 = normal locomotion; 0 = complete hind limb paralysis). Video acquisition of the locomotor performances (5 min) was done with camera (Denver, ACG-8050W) and evaluated

by two independent observers, blinded to the treatment. Individual hind-limb scores were averaged for each animal group at each time point.

SPINAL CORD TRANSCARDIAL PERFUSION

For histological analysis, under deep anesthesia with ketamine hydrochloride (IMALGENE, 100 mg/kg) and medetomidine hydrochloride (DOMITOR, 1 mg/kg), the mice were transcardially perfused with 40 mL of phosphate buffer saline (PBS) 0.1 mol/L, pH 7.4 for 4 min, followed by 50 mL of paraformaldehyde solution (4%) in PBS for 5 min. Spinal cords were carefully removed and post-fixed overnight in the same fixative at 4°C, then transferred to 30% sucrose in 0.1 mol/L phosphate buffer overnight for cryopreservation and stored at 4°C until use.

IMMUNOFLUORESCENCE

The spinal cord was embedded in OCT compound, frozen by immersion in N-pentane at -45°C for 3 minutes, then stored at -80°C until use. Frozen tissues were sectioned at 30 um using a cryostat at -20°C, starting from the rostral edge (about 6 mm rostral to the epicenter), collected in PBS and stored at 4°C until use. Twenty μm thick serial sections (one section every five) were separated and immunofluorescence was done. Sections were incubated with primary antibodies directed against astrocytes (Glial Fibrillary Acidic Protein (GFAP); 1:500 dilution, Millipore) or neurons (NeuN, 1:500 dilution, Millipore) dissolved in PBS, 1% normal goat serum (NGS; Sigma Aldrich) and 0.1% Triton X-100 and incubated overnight at 4°C under constant shaking. Primary antibody staining was detected using secondary antibodies conjugated to fluorophores (Alexa Fluor 647, 1:500; Invitrogen). Spinal cord sections were coverslipped with a 50% glycerol solution in PBS before acquisition at 10X magnification by confocal microscopy (Olympus Fv1000, Laser 594).

COLOCALIZATION STUDY

Study of colocalization was carried out *in vitro* (9-19 cells) and *ex vivo* around the site of injection 1 day post-injury (9 sections, 30 μm thickness, sampled one every two sections, evaluated area 5355 μm^2). Colocalization was quantified by Pearson´s coefficient (Imaris software, Bitplane).

TOTAL NUMBER OF NEURONS IN DAMAGED SPINAL CORD

Acquisition was set using a Cell R microscope (Olympus); Every 5th section (30 um thickness) in a tract of spinal cord of +1.5/-1.3 mm from the injury site was acquired using a 3D mosaic imaging technique with 40x magnification. For frame sampling a grid (200*200 μm) was superimposed on the acquired section and all frames of the grid containing grey matter were examined in a fractioned height of 5 μm. An unbiased counting probe (216*165 μm) was used to count neurons in each frame, with Image j software and a homemade plugin-macro. The total number of neurons was calculated using the formula: $N = \Sigma Q * t/h*1/asf*1/ssf$, where Q is the number of neurons counted in the section, t (section thickness, 30 μm), h (fractionator height, 5 μm), area probe (216*165 μm), area frame (200*200 μm), asf (area probe/area frame), ssf (sampling fraction of every 5th section). The precision of the number of neuronal cells was established by the intra-animal coefficient of error, CE and inter-animal coefficient of variation CV. [38,39] Mean CE: INJ 0.050, NG_Roli 0.044 and CV: INJ 0.283, NG_Roli 0.122.

ASTROCYTOSIS IN SPINAL CORD

The acquisition was set using a Cell R microscope (Olympus). Every 5th section (30 um thickness) in a tract of spinal cord of +1.5/-1.3 mm from the injury site was acquired using a

3D mosaic imaging technique with 40x magnification. For frame sampling a grid (200*200 μm) was superimposed on the acquired section and all frames of the grid containing astrocytes marked with GFAP were examined in a fractioned height of 2 μm. An unbiased counting probe (216*165 μm) was used to quantify $GFAP^+$ staining in each frame, with Image j software and by the Cavalieri method. Volume was calculated as: $V=\sum P*A*T$ (V volume, P number of points hitting white matter, A, grid spacing (200*200 μm) and T, distance between each sampled section (150 μm)). CE and CV were calculated [38,39]: mean CE: INJ 0.067, NG_Roli 0.085. CV: INJ 0.265, NG_Roli 0.285.

STATISTICAL ANALYSES

We used Prism software (Graphpad) for statistical analyses. Mann-Whitney test and one-way ANOVA followed by Bonferroni's post hoc test were used see relative captions.

Acknowledgment.
Authors' research is supported by Politecnico di Milano.

Supporting Information Available:
The Supporting Information is available free of charge via the Internet at http://pubs.acs.org
Scheme of NG synthesis; AFM images of NG-NH_2; FT-IR spectra of NG and NG-NH_2; ^{1}H-NMR (D_2O) spectra of NG and NG-NH_2; NG uptake in untreated, LPS-treated and FGF-IL-4 treated cell of murine astrocytes and microglia, and human astrocytes in vitro; in vitro release profile of Rolipram delivered from NGs; quantitative mRNA analysis of iNOS and Lcn2 expressed by astrocyte cultures after treatment with three factors C1q, IL1α and TNF, (PI) or PI and Rolipram; neuron culture exposed to conditioned medium of untreated astrocytes or conditioned medium of astrocytes pre-incubated for 24h with PI, PI + NG or PI+ Rolipram-loaded NG; neuron culture exposed to conditioned medium of untreated microglia or conditioned medium of LPS or LPS + NG or LPS +Rolipram-loaded NG pre-treated

812 microglia; number of neurons of untreated injured mice compared to Rolipram loaded NG at
813 63 DPI.
814
815
816
817
818
819

SUPPLEMENTARY

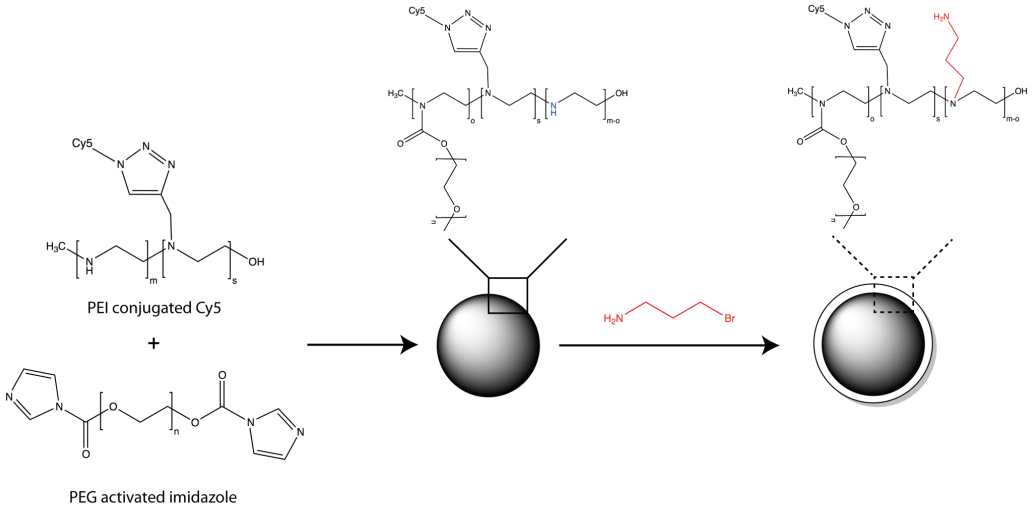

Fig. S1

Scheme of nanogel synthesis. PEI residual amine groups are in blue, and structure of the coating in red.

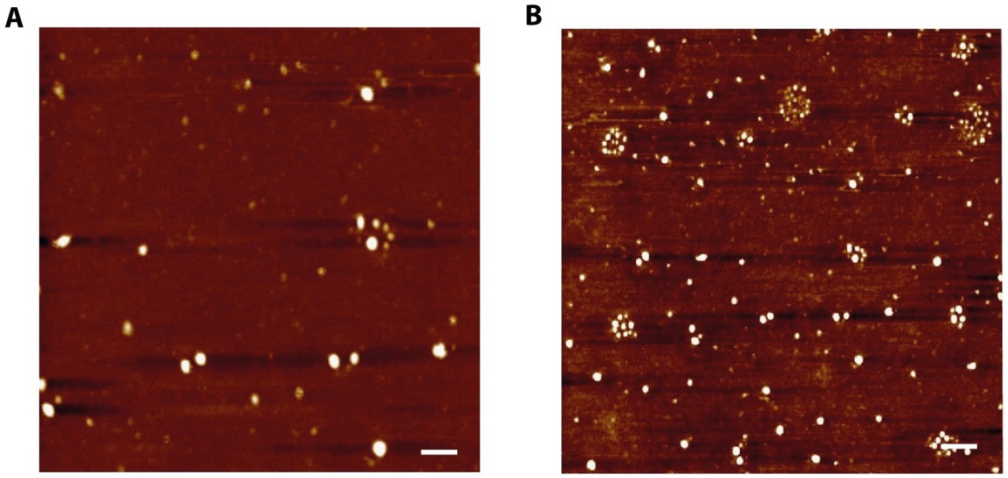

Fig. S2

AFM images of NG-NH_2 (coated nanogels). Scale bars: 500 nm (A), 1000 nm (B).

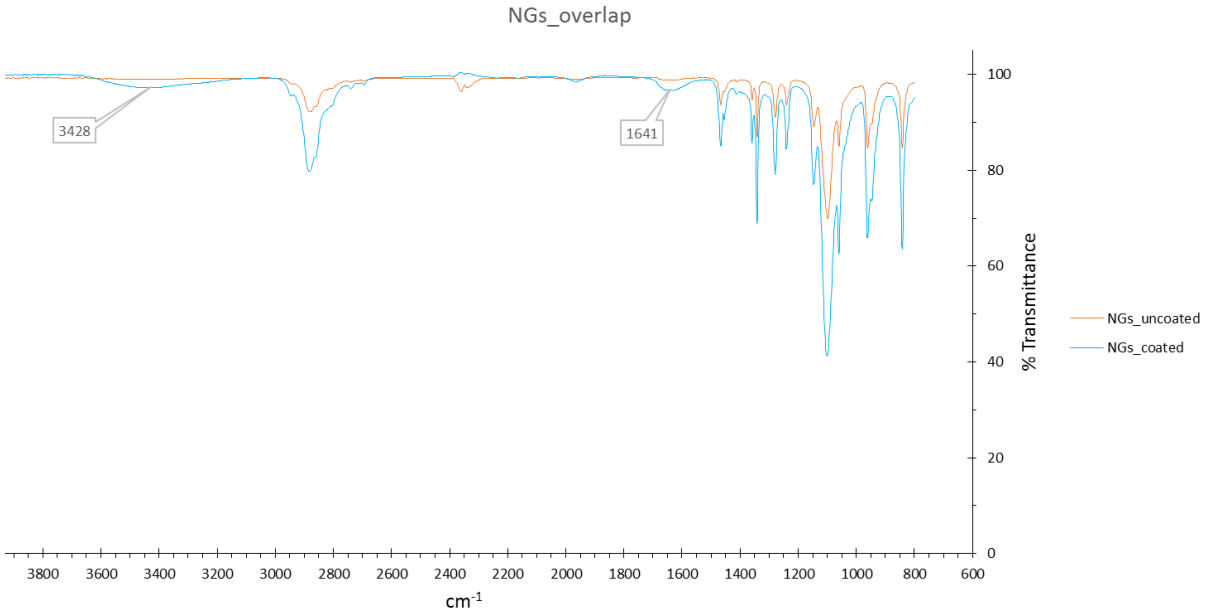

Fig. S3

FT-IR spectra of NG (orange line) and NG-NH_2 (blue line).

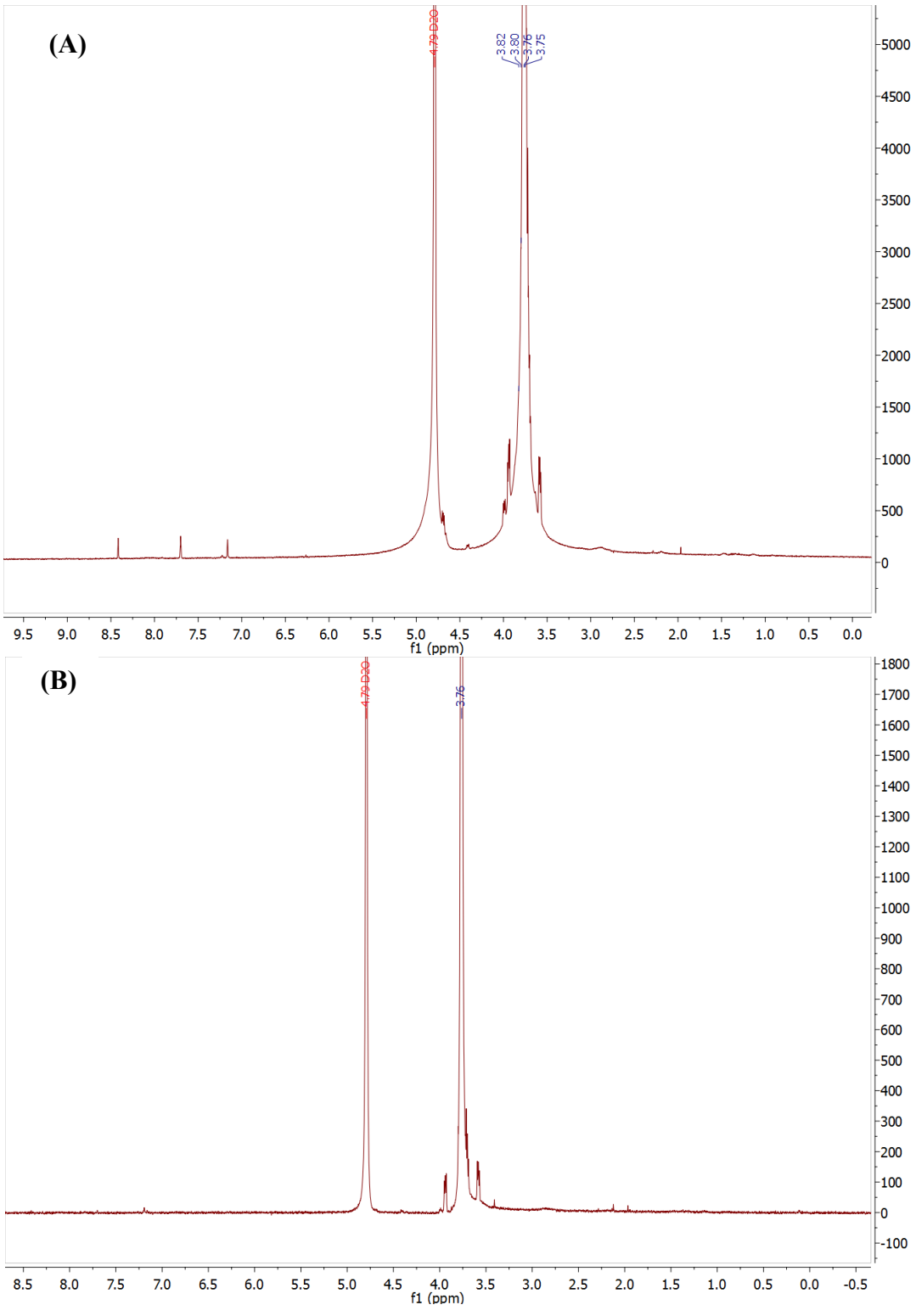

838

839

840

841 ***Fig. S4***

842 *^{1}H-NMR (D_2O) spectra of NG (**A**) and NG-NH_2 (**B**).*

843

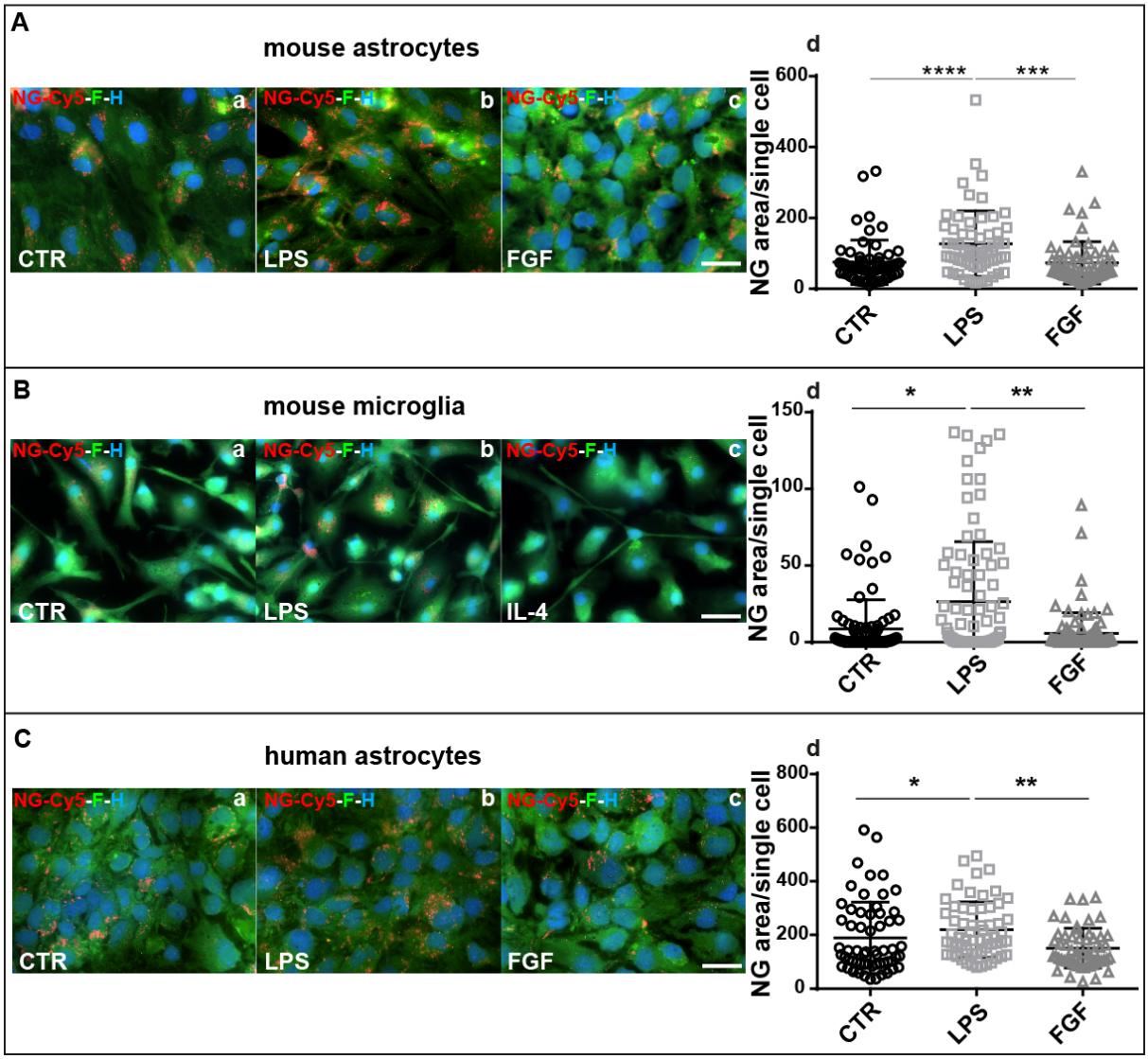

Fig. S5

A) NG uptake in untreated (CTR) (a), LPS-treated (activation stimuli) (b) and FGF (A2 stimuli) (c) treated murine astrocytes in vitro. Quantification of the NG uptake in astrocytes shows higher NG internalization in LPS treated astrocytes compared to CTR and FGF group (d). B) NG uptake in untreated (CTR) (a), LPS-treated (activation stimuli) (b) and IL-4 (M2 stimuli) (c) treated murine microglia in vitro. Quantification of the NG uptake in microglia shows higher NG internalization in LPS treated astrocytes compared to CTR and Il-4 group.

C) NG uptake in untreated (CTR) (a), LPS-treated (activation stimuli) (b) and FGF (A2 stimuli) (c) treated human astrocytes in vitro. Quantification of the NG uptake in astrocytes shows higher NG internalization in LPS treated astrocytes compared to CTR and FGF group (d). Data are mean ± SD. One-way ANOVA followed by Bonferroni's post hoc test. Statistical significance: (*) $p < 0.05$, (**) $p < 0.01$, (***) $p < 0.001$, (****) $p < 0.0001$. Scale bar 10μm.

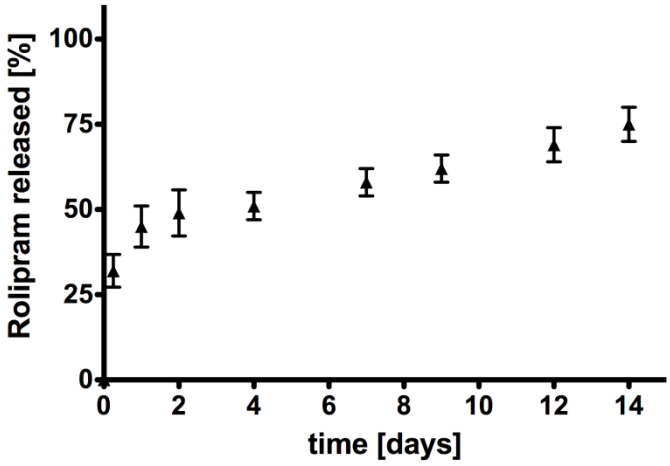

Fig. S6

In vitro release profile of Rolipram delivered from NGs.

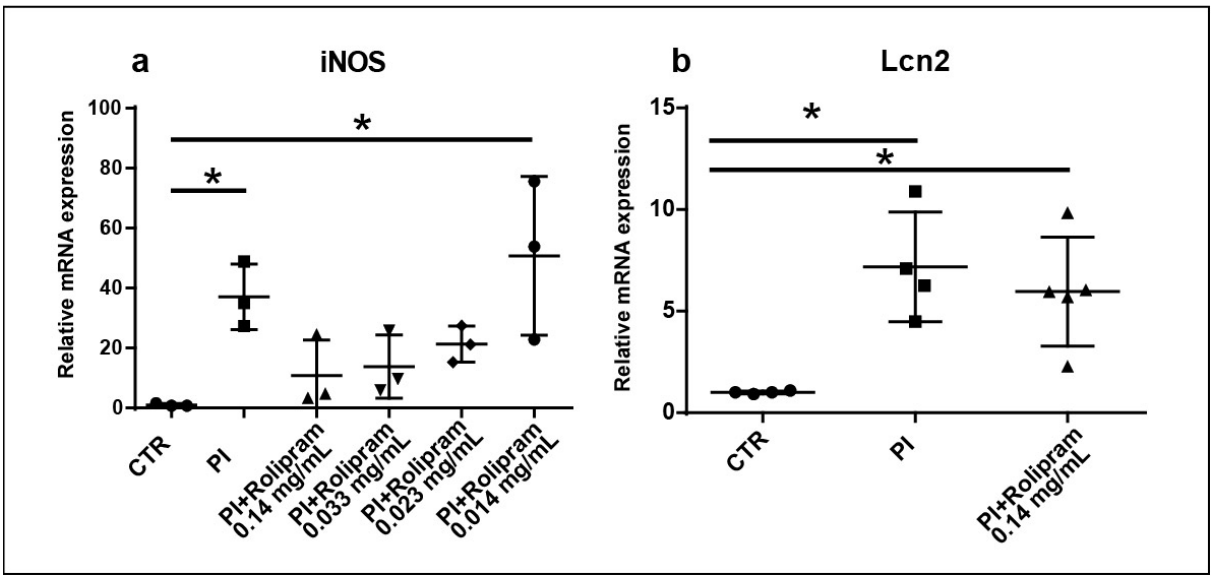

Fig. S7

Quantitative mRNA analysis of iNOS (a) and Lcn2 (b) expressed by astrocyte cultures after treatment with three factors, C1q, IL1α and TNFα (PI) or PI and Rolipram, at the concentrations indicated. Data are mean ± SD. One-way ANOVA followed by Bonferroni's post hoc test. Statistical significance: (*) $p < 0.05$.

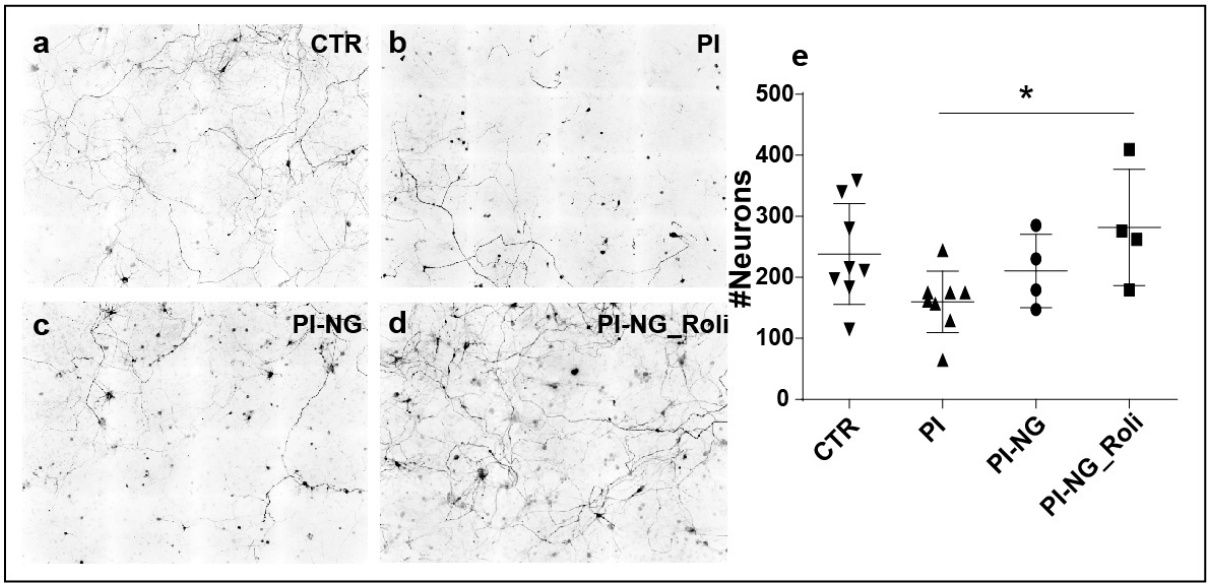

883

884

885 ***Fig.S8***

886 *Neuron culture exposed to conditioned medium of untreated astrocytes (CTR) (a) or*
887 *conditioned medium of astrocytes pre-incubated for 24h with C1q, IL1α and TNFα (PI) (b),*
888 *PI + nanogel (PI-NG) (c), or PI+ Rolipram-loaded nanogel (PI-NG_Roli) (d). Cells are*
889 *stained for SMI32 and quantified by unbiased counting. PI-NG_Roli significantly reversed*
890 *the toxicity of the conditioned medium of PI treated astrocytes, effectively protecting motor*
891 *neurons in vitro (e). Data are mean ± SD. One-way ANOVA followed by Bonferroni's post*
892 *hoc test. Statistical significance: (*) $p < 0.05$.*

893

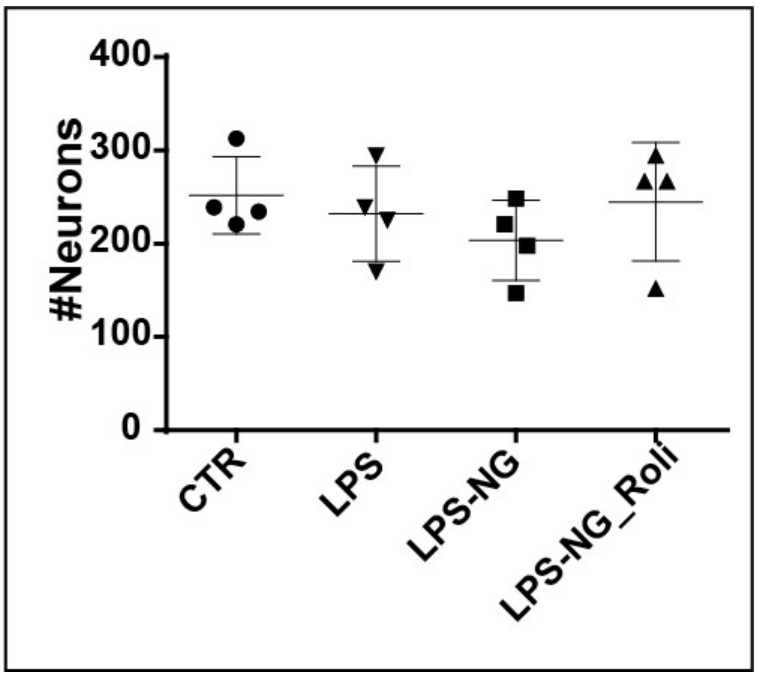

Fig.S9

Neuron culture exposed to conditioned medium of untreated microglia (CTR) or conditioned medium of LPS or LPS + nanogel (LPS-NG) or LPS +Rolipram-loaded nanogel (LPS-NG_Roli) pre-treated microglia. Cells were stained with SMI32 and quantified by unbiased counting. The neuron counts show no significant differences. Data are mean ± SD. One-way ANOVA followed by Bonferroni's post hoc test.

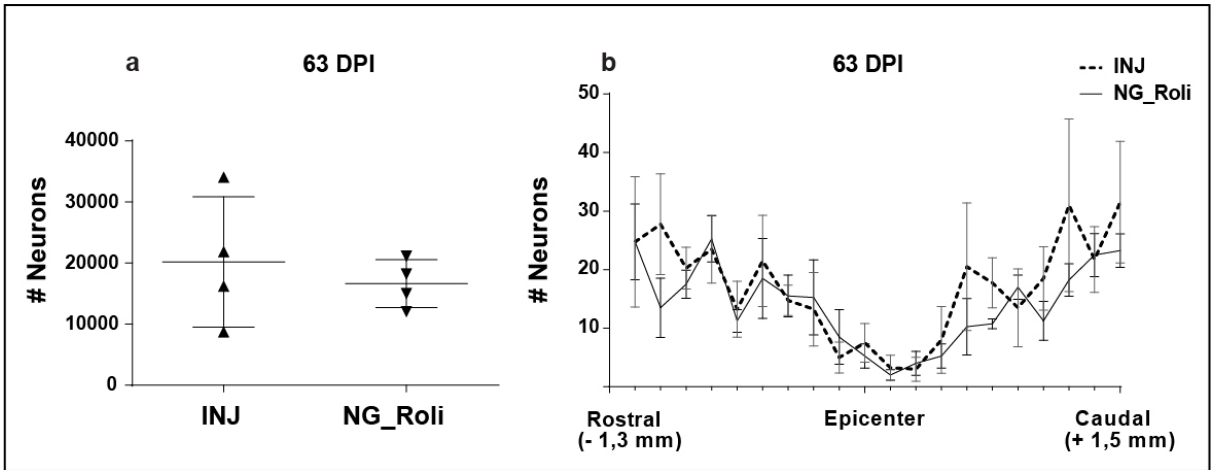

Fig.S10

Number of neurons of untreated injured mice (INJ) compared to Rolipram-loaded NG (NG_Roli) at 63 DPI. We found not significant difference between INJ and NG_Roli mice (a). Graphical representation of neuronal survival in relation to their distance from the injured epicenter at 63 DPI (b).

REFERENCES

(1) Gaudet, A. D.; Fonken, L. K. Glial Cells Shape Pathology and Repair After Spinal Cord Injury. *Neurotherapeutics : the journal of the American Society for Experimental NeuroTherapeutics* **2018**, *15*, 554–577.

(2) Liddelow, S. A.; Barres, B. A. Reactive Astrocytes: Production, Function, and Therapeutic Potential. *Immunity* **2017**, *46*, 957–967.

(3) Liddelow, S. A.; Guttenplan, K. A.; Clarke, L. E.; Bennett, F. C.; Bohlen, C. J.; Schirmer, L.; Bennett, M. L.; Münch, A. E.; Chung, W.-S.; Peterson, T. C. *et al.* Neurotoxic reactive astrocytes are induced by activated microglia. *Nature* **2017**, *541*, 481–487.

(4) Milich, L. M.; Ryan, C. B.; Lee, J. K. The origin, fate, and contribution of macrophages to spinal cord injury pathology. *Acta neuropathologica* **2019**, *137*, 785–797.

(5) Gorshkov, K.; Aguisanda, F.; Thorne, N.; Zheng, W. Astrocytes as targets for drug discovery. *Drug discovery today* **2018**, *23*, 673–680.

(6) Smith, J. A.; Braga, A.; Verheyen, J.; Basilico, S.; Bandiera, S.; Alfaro-Cervello, C.; Peruzzotti-Jametti, L.; Shu, D.; Haque, F.; Guo, P. *et al.* RNA Nanotherapeutics for the Amelioration of Astroglial Reactivity. *Molecular therapy. Nucleic acids* **2018**, *10*, 103–121.

(7) Bradbury, E. J.; Moon, L. D. F.; Popat, R. J.; King, V. R.; Bennett, G. S.; Patel, P. N.; Fawcett, J. W.; McMahon, S. B. Chondroitinase ABC promotes functional recovery after spinal cord injury. *Nature* **2002**, *416*, 636–640.

(8) Lang, B. T.; Cregg, J. M.; DePaul, M. A.; Tran, A. P.; Xu, K.; Dyck, S. M.; Madalena, K. M.; Brown, B. P.; Weng, Y.-L.; Li, S. *et al.* Modulation of the proteoglycan receptor PTPσ promotes recovery after spinal cord injury. *Nature* **2015**, *518*, 404–408.

(9) Siebert, J. R.; Conta Steencken, A.; Osterhout, D. J. Chondroitin sulfate proteoglycans in the nervous system: Inhibitors to repair. *BioMed research international* **2014**, *2014*, 845323.

(10) Vismara, I.; Papa, S.; Rossi, F.; Forloni, G.; Veglianese, P. Current Options for Cell Therapy in Spinal Cord Injury. *Trends in molecular medicine* **2017**, *23*, 831–849.

(11) Papa, S.; Caron, I.; Rossi, F.; Veglianese, P. Modulators of microglia: A patent review. *Expert opinion on therapeutic patents* **2016**, *26*, 427–437.

(12) Caron, I.; Papa, S.; Rossi, F.; Forloni, G.; Veglianese, P. Nanovector-mediated drug delivery for spinal cord injury treatment. *Wiley interdisciplinary reviews. Nanomedicine and nanobiotechnology* **2014**, *6*, 506–515.

(13) Rossi, F.; Perale, G.; Papa, S.; Forloni, G.; Veglianese, P. Current options for drug delivery to the spinal cord. *Expert opinion on drug delivery* **2013**, *10*, 385–396.

(14) Perale, G.; Rossi, F.; Sundstrom, E.; Bacchiega, S.; Masi, M.; Forloni, G.; Veglianese, P. Hydrogels in spinal cord injury repair strategies. *ACS chemical neuroscience* **2011**, *2*, 336–345.

(15) Gao, W.; Borgens, R. B. Remote-controlled eradication of astrogliosis in spinal cord injury via electromagnetically-induced dexamethasone release from "smart" nanowires. *Journal of controlled release : official journal of the Controlled Release Society* **2015**, *211*, 22–27.

(16) Li, X.; Kozielski, K.; Cheng, Y.-H.; Liu, H.; Zamboni, C. G.; Green, J.; Mao, H.-Q. Nanoparticle-mediated conversion of primary human astrocytes into neurons and oligodendrocytes. *Biomaterials science* **2016**, *4*, 1100–1112.

(17) Zhang, H.; Zhai, Y.; Wang, J.; Zhai, G. New progress and prospects: The application of nanogel in drug delivery. *Materials science & engineering. C, Materials for biological applications* **2016**, *60*, 560–568.

(18) Papa, S.; Rossi, F.; Ferrari, R.; Mariani, A.; Paola, M. de; Caron, I.; Fiordaliso, F.; Bisighini, C.; Sammali, E.; Colombo, C. *et al.* Selective nanovector mediated treatment of activated proinflammatory microglia/macrophages in spinal cord injury. *ACS nano* **2013**, *7*, 9881–9895.

(19) Papa, S.; Vismara, I.; Mariani, A.; Barilani, M.; Rimondo, S.; Paola, M. de; Panini, N.; Erba, E.; Mauri, E.; Rossi, F. *et al.* Mesenchymal stem cells encapsulated into biomimetic hydrogel scaffold gradually release CCL2 chemokine in situ preserving cytoarchitecture and promoting functional recovery in spinal cord injury. *Journal of controlled release : official journal of the Controlled Release Society* **2018**, *278*, 49–56.

(20) Kou, L.; Sun, J.; Zhai, Y.; He, Z. The endocytosis and intracellular fate of nanomedicines: Implication for rational design. *Asian Journal of Pharmaceutical Sciences* **2013**, *8*, 1–10.

(21) Oh, N.; Park, J.-H. Endocytosis and exocytosis of nanoparticles in mammalian cells. *International journal of nanomedicine* **2014**, *9 Suppl 1*, 51–63.

(22) Papa, S.; Caron, I.; Erba, E.; Panini, N.; Paola, M. de; Mariani, A.; Colombo, C.; Ferrari, R.; Pozzer, D.; Zanier, E. R. *et al.* Early modulation of pro-inflammatory microglia by minocycline loaded nanoparticles confers long lasting protection after spinal cord injury. *Biomaterials* **2016**, *75*, 13–24.

(23) Anderson, M. A.; Burda, J. E.; Ren, Y.; Ao, Y.; O'Shea, T. M.; Kawaguchi, R.; Coppola, G.; Khakh, B. S.; Deming, T. J.; Sofroniew, M. V. Astrocyte scar formation aids central nervous system axon regeneration. *Nature* **2016**, *532*, 195–200.

(24) Nathan, F. M.; Li, S. Environmental cues determine the fate of astrocytes after spinal cord injury. *Neural regeneration research* **2017**, *12*, 1964–1970.

(25) Zamanian, J. L.; Xu, L.; Foo, L. C.; Nouri, N.; Zhou, L.; Giffard, R. G.; Barres, B. A. Genomic analysis of reactive astrogliosis. *The Journal of neuroscience : the official journal of the Society for Neuroscience* **2012**, *32*, 6391–6410.

(26) Okada, S.; Hara, M.; Kobayakawa, K.; Matsumoto, Y.; Nakashima, Y. Astrocyte reactivity and astrogliosis after spinal cord injury. *Neuroscience research* **2018**, *126*, 39–43.

(27) Rathore, K. I.; Berard, J. L.; Redensek, A.; Chierzi, S.; Lopez-Vales, R.; Santos, M.; Akira, S.; David, S. Lipocalin 2 plays an immunomodulatory role and has detrimental effects after spinal cord injury. *The Journal of neuroscience : the official journal of the Society for Neuroscience* **2011**, *31*, 13412–13419.

(28) Bi, F.; Huang, C.; Tong, J.; Qiu, G.; Huang, B.; Wu, Q.; Li, F.; Xu, Z.; Bowser, R.; Xia, X.-G. *et al.* Reactive astrocytes secrete lcn2 to promote neuron death. *Proceedings of the National Academy of Sciences of the United States of America* **2013**, *110*, 4069–4074.

(29) Conti, A.; Miscusi, M.; Cardali, S.; Germanò, A.; Suzuki, H.; Cuzzocrea, S.; Tomasello, F. Nitric oxide in the injured spinal cord: Synthases cross-talk, oxidative stress and inflammation. *Brain research reviews* **2007**, *54*, 205–218.

(30) Jin, M.; Jang, E.; Suk, K. Lipocalin-2 Acts as a Neuroinflammatogen in Lipopolysaccharide-injected Mice. *Experimental neurobiology* **2014**, *23*, 155–162.

(31) Lee, S.; Park, J.-Y.; Lee, W.-H.; Kim, H.; Park, H.-C.; Mori, K.; Suk, K. Lipocalin-2 is an autocrine mediator of reactive astrocytosis. *The Journal of neuroscience : the official journal of the Society for Neuroscience* **2009**, *29*, 234–249.

(32) Lee, S.; Kim, J.-H.; Kim, J.-H.; Seo, J.-W.; Han, H.-S.; Lee, W.-H.; Mori, K.; Nakao, K.; Barasch, J.; Suk, K. Lipocalin-2 Is a chemokine inducer in the central nervous system: Role of chemokine ligand 10 (CXCL10) in lipocalin-2-induced cell migration. *The Journal of biological chemistry* **2011**, *286*, 43855–43870.

(33) Suk, K. Lipocalin-2 as a therapeutic target for brain injury: An astrocentric perspective. *Progress in neurobiology* **2016**, *144*, 158–172.

(34) Jang, E.; Kim, J.-H.; Lee, S.; Kim, J.-H.; Seo, J.-W.; Jin, M.; Lee, M.-G.; Jang, I.-S.; Lee, W.-H.; Suk, K. Phenotypic polarization of activated astrocytes: The critical role of lipocalin-2 in the classical inflammatory activation of astrocytes. *Journal of immunology (Baltimore, Md. : 1950)* **2013**, *191*, 5204–5219.

(35) Zhang, F.; Lin, Y.-A.; Kannan, S.; Kannan, R. M. Targeting specific cells in the brain with nanomedicines for CNS therapies. *Journal of controlled release : official journal of the Controlled Release Society* **2016**, *240*, 212–226.

(36) Paola, M. de; Mariani, A.; Bigini, P.; Peviani, M.; Ferrara, G.; Molteni, M.; Gemma, S.; Veglianese, P.; Castellaneta, V.; Boldrin, V. *et al.* Neuroprotective effects of toll-like receptor 4 antagonism in spinal cord cultures and in a mouse model of motor neuron degeneration. *Molecular medicine (Cambridge, Mass.)* **2012**, *18*, 971–981.

(37) Yan, Y.; Shin, S.; Jha, B. S.; Liu, Q.; Sheng, J.; Li, F.; Zhan, M.; Davis, J.; Bharti, K.; Zeng, X. *et al.* Efficient and rapid derivation of primitive neural stem cells and generation of brain subtype neurons from human pluripotent stem cells. *Stem cells translational medicine* **2013**, *2*, 862–870.

(38) Cruz-Orive, L. M.; Weibel, E. R. Recent stereological methods for cell biology: A brief survey. *The American journal of physiology* **1990**, *258*, L148-56.

(39) Gundersen, H. J.; Jensen, E. B. The efficiency of systematic sampling in stereology and its prediction. *Journal of microscopy* **1987**, *147*, 229–263.